Inorganic Chemistry
Article
Cite This: Inorg. Chem. XXXX, XXX, XXX−XXX
pubs.acs.org/IC

Xantphos-Capped Pd(II) and Pt(II) Macrocycles of Aryldithiolates: Structural Variation and Catalysis in C−C Coupling Reaction

Pravin A. Mane,[†] Sandip Dey,*[,†,∥] Arup Kumar Pathak,[‡,∥] Mukesh Kumar,[§] and Nattamai Bhuvanesh[⊥]

[†]Chemistry Division, [‡]Theoretical Chemistry Section, and [§]Radiation Biology and Health Science Division, Bhabha Atomic Research Centre, Mumbai-400085, India

[∥]Homi Bhabha National Institute, Training School Complex, Mumbai-400094, India

[⊥]Department of Chemistry, Texas A&M University, P.O. Box 30012, College Station, Texas 77842-3012, United States

Supporting Information

ABSTRACT: The self-assembly of Xantphos-capped $\mathbf{M}(OTf)_2$ ($\mathbf{M}$ = *cis*-$[M'(Xantphos)]^{2+}$; M′ = Pd, Pt) with bridging ligands 1,4-benezenedithiol or 4,4′-biphenyldithiol has been investigated. The reactions have yielded complexes $[\mathbf{M}\{S(C_6H_4)_nSH\}]_2(OTf)_2$ (**I**) and $[\mathbf{M}_2\{S\text{-}(C_6H_4)_nS\}]_2(OTf)_4$ (**II**) (n = 1 or 2). The equilibrium between **I** and **II** has been established in platinum complexes for n = 2, whereas the analogous Pd complex exclusively exist as **II**. These results are different from our previously reported dppe or triethyl phosphine-capped complexes which showed only type **II**. The same reaction with 1,3-benezenedithiol lead to the complex $[\mathbf{M}_2(SC_6H_4SSC_6H_4S)](OTf)_2$ (**III**), containing a S−S bond between two thiolate ligands, formed via a complex of type **I** in solution. Characterization of the complexes was accomplished by NMR spectroscopy, UV−vis spectroscopy and mass spectrometry, and X-ray crystallography. Density functional calculations were performed to estimate the relative stability of three types of complexes. The palladium complexes are excellent catalysts in Suzuki C−C cross coupling reactions under mild conditions, and can be reused eight times without losing significant yield. The activity of the Pd catalysts derived from three dithiol ligand follows opposite trend of the stability as **III** > **II** > **I**. The comparative catalytic activity of the tetranuclear Pd complexes (**II**) of bis-phosphines of varied bite angles, including the structurally characterized $[Pd_2(dppf)_2(SC_{12}H_8S)]_2(OTf)_4$ has also been demonstrated.

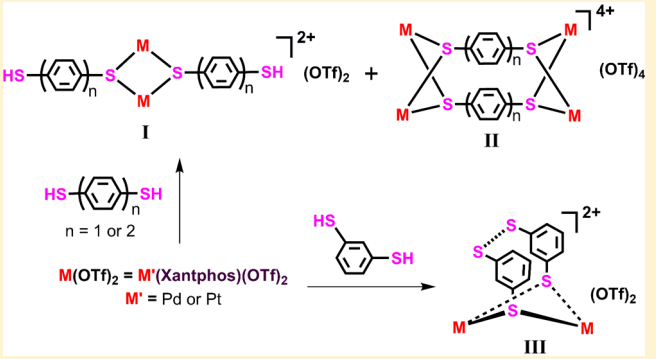

INTRODUCTION

The development of new metallo-supramolecular complexes as functional materials has been of tremendous interest in the past decade. Some of these coordination complexes isolated as discrete molecules have potential uses in drug delivery,[1] enzyme mimics,[2] molecular sensing,[3] guest storage,[4] and homogeneous catalysis.[5−7] The nature of applications depend upon the metal ions and organic ligands used, capable of showing noncovalent interactions, as well as the rigidity, size of cavity, charge and solubility of the supramolecular complexes. Among the transition metals, Pd(II) and Pt(II) ions have been widely exploited in the construction of metallo-supramolecular assembly owing to their square-planar geometry and higher stability over the main group metals, which generally show unpredictable geometry. The final structure obviously depends on the bonding mode of building blocks, thermodynamic stability, entropy change, steric factor and many more.[8] Employing a large number of bis-pyridyl ligands of varying spacer group, by incorporating organic group,[1−6,8] or heteroatom in the ligand backbone,[9,10] a library of fascinating structures were generated containing metal−pyridyl bond. A few such Pt complexes have been recently explored as functional materials to generate chiral metallogels,[11] stabilizer for G-quadruplexes,[12] and antitumor agent.[13] The self-assembled Pd_6 compound from triimidazole or oxadiazole ligand has been established as catalysts in Diels−Alder[14] or Suzuki coupling reactions.[15]

However, the thiolate ligand (RS^-), capable of forming rigid structures owing to stronger metal−sulfur bond, is under explored in the construction of metallo-supramolecular complexes. It may be due to the tendency of the ligand to form sparingly soluble oligomer or polymer rather than the discrete molecules. We have recently reported the supramolecular assemblies of Pd(II) and Pt(II) complexes using mercaptobenzoic acid[16] via intermolecular H-bonding and aryl dithiolate ligands[7] via coordinate bond. The macrocyclic palladium complexes, $[Pd_2(dppe)_2\{S(C_6H_4)_nS\}]_2(OTf)_4$ and

Received: September 27, 2018

DOI: 10.1021/acs.inorgchem.8b02726
Inorg. Chem. XXXX, XXX, XXX−XXX

$[Pd_2(dppe)_2(SCH_2C_6H_4CH_2S)]_4(OTf)_8$ (n = 1, 2; dppe = 1,2-bis(diphenylphosphino)ethane) showed excellent catalytic activity in Suzuki[7] and Heck[17] C−C coupling reactions. Encouraged by these results we decided to investigate the effect of wide-bite-angle phosphine, Xantphos (9,9-dimethyl-4,5-bis(diphenylphosphino)xanthenes), as capping ligand on the structures as well as the catalytic activity of the resulted complexes derived from the same dithiol ligands. The capping ligand strongly influences the nuclearity and structures of the self-assembled products particularly in solution.[18,19] It is well-established that the large bite angle of diphosphine has positive influence on the catalytic activity of Pd complexes in various C−C,[20] C−N,[21,22] and C−O[23] bond forming reactions. The wide bite angle and flexible coordination environment of Xantphos[24] are factors responsible for making it highly efficient ligand among other large bite angle diphosphines such as DPEphos (bis(2-diphenylphosphinophenyl)ether), dppf (1,1′-bis(diphenylphosphino)ferrocene), or Binap (2,2′-bis-(diphenylphosphino)-1,1′-binaphthyl) in catalysis reactions.[25,26]

We have investigated the reactions of $[M'(Xantphos)(OTf)_2]$ and arylenedithiols of varying position of thiol groups as bridging ligands (Scheme 1). Interestingly, the ^{31}P NMR

Scheme 1. Aryldithiol and Diphosphine Ligands with Bite Angles in Degree[a]

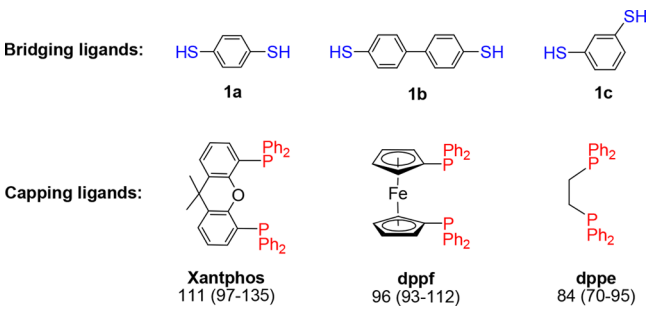

[a]Flexibility range in parentheses.

spectrum of the resulted Pd and Pt complexes showed two distinct signals indicating the presence of two species in solution. One of the dithiolate complex, $[M'_2(Xantphos)_2\{S(C_6H_4)_nS\}]_2(OTf)_4$, is similar to the dppe analogue[7] which was earlier isolated as a single product, whereas the other is identified as dinuclear complex containing free thiol group, $[M'(Xantphos)\{S(C_6H_4)_nSH\}]_2(OTf)_2$. The same reaction with 1,3-benezenedithiol lead to the complex $[M'_2(Xantphos)_2(SC_6H_4SSC_6H_4S)](OTf)_2$ containing a S−S bond. The performance of the catalytic activity of the isolated Pd complexes was evaluated in Suzuki C−C coupling reactions in details. Moreover, a new complex of another large bite angle diphosphine dppf was also prepared. Under optimized reaction conditions, i.e., reflux in methanol, the comparative activity of the tetranuclear complexes $[Pd_2(P^{\frown}P)_2(SC_{12}H_8S)]_2(OTf)_4$ of varied bite angles and flexibility range[27,28] of P^P = Xantphos, dppf, and dppe has been evaluated (Scheme 1).

EXPERIMENTAL SECTION

2a, Pd(Xantphos)(OTf)$_2$. To a dichloromethane solution of (25 mL) of Pd(Xantphos)Cl_2 (301 mg, 0.39 mmol), solid AgOTf (307 mg, 1.19 mmol) was added. The reaction mixture was stirred for 16 h with exclusion of light; the solvent was filtered and concentrated to 10 mL. Diethyl ether (25 mL) was added to precipitate yellow solid which was recrystallized from dichloromethane−ether mixture to yield yellow crystals of **2a** (305 mg, 78%; mp 145 °C (dec)). Anal. Calcd for $C_{41}H_{32}F_6O_7P_2PdS_2\cdot(CH_2Cl_2)_{0.5}(H_2O)_{3.5}$: C, 45.78; H, 3.70; S, 5.89. Found: C, 45.28; H, 3.49; S, 5.69%. ^1H NMR (300 MHz, $CDCl_3$): δ 1.95 (s, 6H, CH_3), 7.18−7.25 (m, 10H, m-H of PPh_2 + CHC*H*CH), 7.33−7.42 (m, 14H, o-H/p-H of PPh_2 + CPC*H*CH), 7.91 (d, $^3J_{HH}$ = 7.8 Hz, 2H, CHC*H*CC), $^{31}P\{^1H\}$ NMR (121 MHz, $CDCl_3$): δ 26.6 (s). UV/vis (acetone): λ_{max} (ε in M^{-1} cm^{-1}) 329(9515) nm.

2b, Pt(Xantphos)(OTf)$_2$. Prepared in a manner similar to that for **2a**, using Pt(Xantphos)Cl_2 (432 mg, 0.51 mmol) and AgOTf (394 mg, 1.53 mmol) to give colorless solid which was recrystallized from dichloromethane−hexane mixture to yield colorless crystals of **2b** (498 mg, 91%; mp 172 °C (dec)). Anal. Calcd for $C_{41}H_{32}F_6O_7P_2PtS_2\cdot(H_2O)_2$: C, 44.45; H, 3.28; S, 5.79. Found: C, 44.71; H, 3.36; S, 5.66%. ^1H NMR (300 MHz, $CDCl_3$): δ 1.94 (s, 6H, CH_3), 7.17−7.22 (m, 10H, m-H of PPh_2 + CHC*H*CH), 7.32−7.39 (m, 14H, o-H/ p-H of PPh_2 + CPC*H*CH), 7.87 (d, $^3J_{HH}$ = 7.8 Hz, 2H, CHC*H*CC). $^{31}P\{^1H\}$ NMR (121 MHz, $CDCl_3$): δ −4.4 (s, $^1J_{Pt-P}$ = 4132 Hz). UV/vis (acetone): λ_{max} (ε in M^{-1} cm^{-1}) 327(1266) nm.

3a, [Pd(Xantphos)(1,4-SC$_6$H$_4$SH)]$_2$(OTf)$_2$ (I) and [Pd$_2$(Xantphos)$_2$(1,4-SC$_6$H$_4$S)]$_2$(OTf)$_4$ (II). To an acetone solution of (5 mL) of **1a** (5.4 mg, 0.038 mmol), acetone solution (5 mL) of **2a** (75.2 mg, 0.076 mmol) was added. The wine-red solution was stirred for 4 h. The solvent was evaporated in vacuuo; the red residue was washed with diethyl ether and extracted with acetone (3 × 5 mL). Diethyl ether (10 mL) was added to yield red colored solid of **3a** (48.1 mg, 0.024 mmol, 65%; mp >230 °C (dec)). Anal. Calcd for **3a-I**$\cdot(H_2O)_2$ $C_{92}H_{74}F_6O_8P_4Pd_2S_6\cdot(H_2O)_2$: C, 55.64; H, 3.96; S, 9.67%. Calcd for **3a-II**$\cdot(H_2O)_4$ $C_{172}H_{136}F_{12}O_{16}P_8Pd_4S_8\cdot(H_2O)_4$: C, 56.00; H, 3.93; S, 6.95%. Found: C, 55.11; H, 3.75; S, 9.98%. Calcd for **3a-I**: Pd, 10.91%. Calcd for **3a-II**: Pd, 11.77%. Found: Pd, 12.00%. ^1H NMR (300 MHz, acetone-d_6): δ 1.50 (s, 6H, CH_3), 1.97 (s, 6H, CH_3), 5.60 (br s, 4H, C_6H_4), 6.88 (br s, 12H, p-H of PPh_2 + CHC*H*CH), 7.39 (m, 20H, m-H of PPh_2 + CPC*H*CH), 7.66 (br s, 16H, o-H of PPh_2), 7.92 (br s, 4H, CHC*H*CC), ^1H NMR (500 MHz, CD_3OD): δ 1.50 (s, 6H, CH_3), 1.97 (s, 6H, CH_3), 5.53 (br s, 8H, C_6H_4), 6.84 (br s, 12H, p-H of PPh_2 + CHC*H*CH), 7.29 (m, 20H, m-H of PPh_2 + CPC*H*CH), 7.59 (br s, 16H, o-H of PPh_2), 7.90 (br s, 4H, CHC*H*CC). $^{31}P\{^1H\}$ NMR (121 MHz, acetone-d_6): δ 4.3 (br, s), 7.9 (br, s) in ∼1:1 ratio. $^{31}P\{^1H\}$ NMR (243 MHz, CD_3OD): δ 5.1 (br, s), 12.8 (br, s) in ∼1:1 ratio. Electrospray ionization mass spectrometry (ESI-MS; ion, relative intensity): m/z 1168.1 ($[Pd_3(Xantphos)_3(SC_6H_4SH)_2 + 2H]^{2+}$, 2%), 1165.1 ([**3a-II** + H − (3OTf + Pd(Xantphos) + $2C_6H_4$)]$^{2+}$, 1%), 825.1 ([**3a-I** − (2OTf + Pd(Xantphos)(SC_6H_4SH))]$^+$, 7%), 759.1 ([Pd(Xantphos)S + 2H + CH_3CN]$^+$, 10%), 754.1 ([**3a-II** − (4OTf + $Pd_2(Xantphos)_2(SC_6H_4S)$)]$^{2+}$, 5%), 710.0 ([Pd(Xantphos)(SC_6H_4)$_2$ + CH_3CN − $3C_6H_5$]$^+$, 100%), 685.1 ([Pd(Xantphos) + H]$^+$, 7%). UV/vis (acetone): λ_{max} (ε in M^{-1} cm^{-1}) 350(28123), 397(sh, 15883), 503(17707) nm.

3b, [Pd$_2$(Xantphos)$_2$(4,4′-SC$_{12}$H$_8$S)]$_2$(OTf)$_4$ (II). Prepared in a manner similar to that for **3a**, using **2a** (75.1 mg, 0.076 mmol) and **1b** (8.3 mg, 0.038 mmol) to yield the title complex as red solid (50.3 mg, 0.013 mmol, 70%; mp > 230 °C (dec)). Anal. Calcd for **3b** $C_{184}H_{144}F_{12}O_{16}P_8Pd_4S_8$: C, 58.63; H, 3.85; S, 6.81. Found: C, 58.60; H, 3.82; S, 6.94%. ^1H NMR (300 MHz, acetone-d_6): δ 1.62 (s, 6H, CH_3), (another peak due to the methyl group merged with the solvent peak at δ 2.05 ppm), 5.89 (d, $^3J_{HH}$ = 7.8 Hz, 4H, o-H, $C_{12}H_8$), 6.32 (d, $^3J_{HH}$ = 7.8 Hz, 4H, m-H, $C_{12}H_8$), 7.09 (br s, 4H, CHC*H*CH), 7.22 (br s, 8H, p-H of PPh_2), 7.30−7.49 (m, 20H, m-H of PPh_2 + CPC*H*CH), 7.53 (t, $^3J_{HH}$ = 6.9 Hz, 16H, o-H of PPh_2), 7.97 (d, $^3J_{HH}$ = 7.8 Hz, 4H, CHC*H*CC). ^1H NMR (500 MHz, CD_3OD): δ 1.56 (s, 6H, CH_3), 2.01 (s, 6H, CH_3), 5.84 (d, $^3J_{HH}$ = 8.0 Hz, 4H, o-H, $C_{12}H_8$), 6.22 (d, $^3J_{HH}$ = 8.0 Hz, 4H, m-H, $C_{12}H_8$), 7.01 (br s, 4H, CHC*H*CH), 7.14 (br s, 8H, p-H of PPh_2), 7.31−7.44 (m, 20H, m-H of PPh_2 + CPC*H*CH), 7.53 (t, $^3J_{HH}$ = 7.5 Hz, 16H, o-H of PPh_2), 7.89 (d, $^3J_{HH}$ = 7.5 Hz, 4H, CHC*H*CC). $^{13}C\{^1H\}$ NMR (201 MHz, acetone-d_6): δ 23.4 (s, CH_3), 38.7 (s, CCH_3), 117.6 (d, $^1J_{PC}$ = 45.1 Hz, CP of $C_{15}H_{12}O$), 127.4 (s, o-C of $C_{12}H_8$), 127.9 (s, CH of

DOI: 10.1021/acs.inorgchem.8b02726
Inorg. Chem. XXXX, XXX, XXX−XXX

$C_{15}H_{12}O$), 130.3 (s, *m*-C of $C_{12}H_8$), 130.5 (s, CH of $C_{15}H_{12}O$), 130.8 (s, *m*-C of C_6H_5), 131.8 (s, CS of $C_{12}H_8$), 132.9 (d, $^1J_{PC}$ = 71.6 Hz, CP of C_6H_5), 134.2 (s, *o*-/*p*-C of C_6H_5), 134.7 (s, CH of $C_{15}H_{12}O$), 137.6 (s, *C*C of $C_{12}H_8$), 139.0 (s, CCC(CH_3) of $C_{15}H_{12}O$), 157.4 (s, *C*O of $C_{15}H_{12}O$). $^{19}F\{^1H\}$ NMR (376 MHz, acetone-d_6): δ −78.7 (s). $^{31}P\{^1H\}$ NMR (121 MHz, acetone-d_6): δ 9.1 (s). ESI-MS (ion, relative intensity): *m*/*z* 901.1 ([**3b-II** − (4OTf + Pd_2(Xantphos)$_2$)]$^{2+}$, 13%), 832.1 ([Pd(Xantphos)S_2 + 2CH_3CN + 2H]$^+$, 7%), 816.6 ([Pd_2(Xantphos)$_2$S(OTf) + 2CH_3CN + 2H]$^{+2}$, 9%), 719.1 ([Pd(Xantphos)($SC_{12}H_8$) + 2CH_3CN − 3C_6H_5]$^+$, 22%), 710.0 ([Pd(Xantphos)(SC_6H_4)$_2$ + CH_3CN − 3C_6H_5]$^+$, 100%), 395.0 ([Pd_2(Xantphos)]$^{2+}$, 24%). UV/vis (acetone): λ_{max} (ε in M^{-1} cm^{-1}) 344(41063), 395(sh, 27590), 518(28950) nm.

3c, [Pd(Xantphos)(1,3-SC$_6$H$_4$SH)]$_2$(OTf)$_2$ (I′) and [Pd$_2$(Xantphos)$_2$(1,3-SC$_6$H$_4$SSC$_6$H$_4$S)](OTf)$_2$ (III). Prepared in a manner similar to that for **3a**, using **2a** (106.4 mg, 0.108 mmol) and **1c** (15.5 mg, 0.109 mmol) to give a red colored solid [(68.5 mg, 0.035 mmol, 65%; mp > 230 °C (dec)). Anal. Calcd for $C_{92}H_{70}F_6O_8P_4Pd_2S_6$: C, 56.65; H, 3.82; S, 9.86. Found: C, 56.11; H, 3.59; S, 8.83%. ^1H NMR (600 MHz, acetone-d_6): δ 1.83 (br s, CH_3), 1.88 (s, CH_3), 6.38−8.22 (m, $C_{15}H_{12}O$ + PPh_2 + C_6H_4). $^{31}P\{^1H\}$ NMR (243 MHz, acetone-d_6): δ 15.9 (s), 18.5 (br s), 27.0 (s)], which on recrystallization from acetone-hexane mixture at −5 °C to yield orange crystals of **3c** (34.8 mg, 0.017 mmol, 33%; mp > 200 °C (dec)). Anal. Calcd for $C_{92}H_{72}F_6O_8P_4Pd_2S_6$: C, 56.70; H, 3.72; S, 9.87. Found: C, 56.46; H, 3.70; S, 9.57%. ^1H NMR (600 MHz, acetone-d_6): δ 1.43 (s, 6H, CH_3), 1.68 (s, 6H, CH_3), 5.19 (d, $^3J_{HH}$ = 7.8 Hz, 2H, C_6H_4), 6.31 (br s, 2H, C_6H_4), 6.78 (t, $^3J_{HH}$ = 7.8 Hz, 2H, C_6H_4), 6.87 (br m, 20H, *m*-H of PPh_2 + C_6H_4 + CHC*H*CH), 7.02 (br, 4H, *p*-H of PPh_2), 7.09 (m, 4H, *p*-H of PPh_2), 7.24 (d, $^3J_{HH}$ = 7.8 Hz, 2H, CHC*H*CH), 7.30−8.25 (br m, 24H, *o*-H of PPh_2 + $C_{15}H_{12}O$). $^{31}P\{^1H\}$ NMR (243 MHz, acetone-d_6): δ 22.5 (s). UV/vis (acetone): λ_{max} (ε in M^{-1} cm^{-1}) 353(20159), 430(14269), 461(sh, 10458) nm.

3d, [Pd(Xantphos)(1,4-SCH$_2$C$_6$H$_4$CH$_2$SH)]$_2$(OTf)$_2$ and [Pd$_2$(Xantphos)$_2$(1,4-SCH$_2$C$_6$H$_4$CH$_2$S)]$_m$(OTf)$_{2m}$. Prepared in a manner similar to that for **3a**, using **2a** (70.9 mg, 0.072 mmol) and **1d** (6.1 mg, 0.035 mmol) to yield the title complex as orange solid (42.5 mg, 0.005 mmol, 62%; mp 202 °C). Anal. Calcd for [Pd(Xantphos)($SCH_2C_6H_4CH_2SH$)]$_2$(OTf)$_2$ $C_{96}H_{82}F_6O_8P_4Pd_2S_6$: C, 57.46; H, 4.12; S, 9.59. Found: C, 57.96; H, 4.23; S, 8.94%. ^1H NMR (300 MHz, acetone-d_6): δ 1.63 (br s, 6H, CH_3), (another peak due to the methyl group merged with the solvent peak at δ 2.05 ppm), 3.28 (s, 8H, SCH_2), 6.45−8.45 (br m, 60H, Xantphos + C_6H_4). $^{31}P\{^1H\}$ NMR (121 MHz, acetone-d_6): δ 10.8 (br s), 12.9 (br s) in ∼1:1 ratio.

4a, [Pt(Xantphos)(1,4-SC$_6$H$_4$SH)]$_2$(OTf)$_2$ (I) and [Pt$_2$(Xantphos)$_2$(1,4-SC$_6$H$_4$S)]$_2$(OTf)$_4$ (II). An acetone solution (5 mL) of **2b** (100.1 mg, 0.093 mmol) was added to a methanolic solution (5 mL) of **1a** (6.6 mg, 0.046 mmol) with stirring which continued for 24 h. The solvent was evaporated in vacuuo; the red residue was washed with hexane and extracted with acetone (3 × 5 mL). A few drops of hexane were added to yield yellow crystal of **4a** (71.3 mg, 0.033 mmol, 72%; mp > 230 °C (dec)). Anal. Calcd for **4a-I** $C_{92}H_{74}F_6O_8P_4Pt_2S_6$: C, 51.93; H, 3.51; S, 9.04. Calcd for **4a-II** $C_{172}H_{136}F_{12}O_{16}P_8Pt_4S_8$: C, 52.02; H, 3.45; S, 6.46. Found: C, 52.02; H, 3.65; S, 8.85%. ^1H NMR (500 MHz, acetone-d_6): δ 1.52 (s, 6H, CH_3), 2.00 (s, 6H, CH_3), 5.30 (br s, 4H, C_6H_4), 5.98 (br s, 4H, C_6H_4), 6.20−8.25 (br m, 48H, Ph + $C_{15}H_{12}O$), 8.91 (br, 4H, $C_{15}H_{12}O$). $^{31}P\{^1H\}$ NMR (121 MHz, acetone-d_6): δ −1.46 (s, $^1J_{Pt-P}$ = 3505 Hz), −8.52 (s, $^1J_{Pt-P}$ = 3365 Hz). ESI-MS (ion, relative intensity): *m*/*z* 1299.7 ([**4a-II** − (4OTf + Pt(Xantphos))]$^{2+}$, 8%), 1255.7 ([**4a-II** + 4CH_3CN + H − (Xantphos + 4C_6H_5 + SC_6H_4S)]$^{2+}$, 2%), 1173.8 ([**4a-II** − 3OTf]$^{3+}$, 100%), 1132.8 ([**4a-II** − (2OTf + Pt + C_6H_5)]$^{3+}$, 15%), 914.1 ([**4a-I** − (2OTf + [Pt(Xantphos)(SC_6H_4SH)]$^+$, 2%), 843.1 ([Pt_2(Xantphos)$_2$(SC_6H_4S)]$^{2+}$, 20%). UV/vis (acetone): λ_{max} (ε in M^{-1} cm^{-1}) 332(22172), 366(sh, 15763), 447(5577) nm.

4b, [Pt(Xantphos)(4,4′-SC$_{12}$H$_8$SH)]$_2$(OTf)$_2$ (I) and [Pt$_2$(Xantphos)$_2$(4,4′-SC$_{12}$H$_8$S)]$_2$(OTf)$_4$ (II). Prepared in a manner similar to that for **4a**, using **2b** (48.1 mg, 0.045 mmol) and **1b** (4.9 mg, 0.022 mmol) and recrystallized from acetone−hexane mixture to yield yellow crystals of **4b** (36.1 mg, 0.008 mmol, 78%; mp > 230 °C (dec)). Anal. Calcd for **4b-II** $C_{184}H_{144}F_{12}O_{16}P_8Pt_4S_8$: C, 53.59; H, 3.52; S, 6.22. Found: C, 53.87; H, 4.08; S, 5.64%. ^1H NMR (300 MHz, acetone-d_6): δ 1.58 (s, 6H, CH_3), another peak correspondence to the methyl group merged with the solvent peak at δ 2.05 ppm, 5.77 (br s, 4H, *o*-H, $C_{12}H_8$), 6.28 (br s, 4H, *m*-H, $C_{12}H_8$), 7.12 (br s, 4H, CHC*H*CH), 7.24 (br s, 8H, *p*-H of PPh_2), 7.34−7.54 (m, 36H, *o*-H/*m*-H of PPh_2 + CPC*H*CH), 7.98 (d, $^3J_{HH}$ = 7.2 Hz, 4H, CHC*H*CC). ^1H NMR (500 MHz, CD_3OD): δ 1.53 (s, 6H, CH_3), 2.01 (S, 6H, CH_3), 5.81 (br s, 4H, *o*-H, $C_{12}H_8$), 6.26 (br s, 4H, *m*-H, $C_{12}H_8$), 6.97 (br s, 4H, CHC*H*CH), 7.11 (br s, 8H, *p*-H of PPh_2), 7.27−7.60 (m, 36H, *o*-/*m*-H of PPh_2 + CPC*H*CH), 7.89 (br s, 4H, CHC*H*CC). $^{13}C\{^1H\}$ NMR (201 MHz, acetone-d_6): δ 22.9 (s, CH_3), 39.1 (s, *C*CH_3), 116.2 (d, $^1J_{PC}$ = 57.5 Hz, CP of $C_{15}H_{12}O$), 127.4 (s, *o*-C of $C_{12}H_8$), 130.1 (s, *m*-C of $C_{12}H_8$), 130.5 (s, CH of $C_{15}H_{12}O$), 130.7 (s, *m*-C of C_6H_5), 131.6 (br s, CS of $C_{12}H_8$), 133.1 (d, $^1J_{PC}$ = 77.0 Hz, CP of C_6H_5), 134.2 (s, CH of $C_{15}H_{12}O$), 134.5 (s, *o*-C of C_6H_5), 138.4 (br s, *C*C of $C_{12}H_8$), 138.9 (s, CCC(CH_3) of $C_{15}H_{12}O$), 158.1 (s, *C*O of $C_{15}H_{12}O$), the peaks due to one CH group of $C_{15}H_{12}O$ and *p*-C of C_6H_5 are merged with the peaks at δ 130.1 and 134.5 ppm, respectively. $^{31}P\{^1H\}$ NMR (121 MHz, acetone-d_6): δ −0.89 (br s, $^1J_{Pt-P}$ = 3380 Hz). ESI-MS (ion, relative intensity): *m*/*z* 1911.3 ([**4b-II** − 2OTf]$^{2+}$, 9%), 1375.7 ([**4b-II** − (4OTf + Pt(Xantphos))]$^{2+}$, 1%), 1224.5 ([**4b-II** − 3OTf]$^{3+}$, 100%), 881.2 ([**4b-II** − 4OTf]$^{4+}$, 88%). UV/vis (acetone): λ_{max} (ε in M^{-1} cm^{-1}) 328(33457), 341(sh, 27427), 411(32383) nm.

4c, [Pt(Xantphos)(1,3-SC$_6$H$_4$SH)]$_2$(OTf)$_2$ (I′) and [Pt$_2$(Xantphos)$_2$(1,3-SC$_6$H$_4$SSC$_6$H$_4$S)](OTf)$_2$ (III). Prepared in a manner similar to that for **4a**, using **2b** (61.2 mg, 0.057 mmol) and **1c** (8.1 mg, 0.056 mmol) and recrystallized from acetone−hexane mixture to yield yellow powder [(44.1 mg, 0.020 mmol, 73%; mp 221 °C (dec)). Anal. Calcd for $C_{46}H_{37}F_3O_4P_2PtS_3$: C, 51.93; H, 3.51; S, 9.04. Found: C, 51.35; H, 3.32; S, 8.75%. ^1H NMR (600 MHz, acetone-d_6): δ 1.85 (s, 6H, CH_3), 2.20 (s, 6H, CH_3), 3.99 (d, $^3J_{HH}$ = 7.8 Hz, 2H, C_6H_4), 5.10 (t, $^3J_{HH}$ = 7.8 Hz, 2H, C_6H_4), 5.28 (d, $^3J_{HH}$ = 9.6 Hz, 2H, C_6H_4), 6.47, 7.06 (dt, $^3J_{HH}$ (t) = 7.8 Hz, $^4J_{PH}$ (d) = 2.4 Hz, 8H, *p*-H of PPh_2), 6.88−7.06, 7.57−7.82 (m, 32H, *m*-/*o*-H of PPh_2), 7.14, 8.04 (each t, $^3J_{HH}$ = 8.4 Hz, 4H, CHC*H*CH), 8.15 (d, $^3J_{HH}$ = 8.4 Hz, 2H, CPC*H*CH, another peak for the same group has been merged with peak of Ph), 8.24, 8.26 (each d, *J* = 9.0 Hz, 4H, CHC*H*CC). $^{31}P\{^1H\}$ NMR (243 MHz, acetone-d_6): δ 7.5 (d, $^2J_{PP}$ = 24 Hz, $^1J_{Pt-P}$ = 3057 Hz), 18.1 (d, $^2J_{PP}$ = 24 Hz, $^1J_{Pt-P}$ = 2902 Hz)]. The yellow solid redissolved in minimum quantity of acetone, a few drops of hexane were added to yield a reddish solid with few crystals of **3c** (21.8 mg, 0.010 mmol, 36%; mp > 250 °C (dec)). Anal. Calcd for $C_{92}H_{74}F_6O_8P_4Pt_2S_6$: C, 51.93; H, 3.51; S, 9.04. Found: C, 51.23; H, 3.48; S, 8.73%. ^1H NMR (600 MHz, acetone-d_6): δ 1.31 (s, 6H, CH_3), (another peak due to the methyl group merged with the solvent peak at δ 2.05 ppm), 4.74 (br s, 2H, C_6H_4), 5.10 (br s, 2H, C_6H_4), 6.54 (br s, 2H, C_6H_4), 6.65−7.63 (m, 40H, PPh_2), 7.77 (t, $^3J_{HH}$ = 7.8 Hz, 4H, CHC*H*CH), 7.94 (br s, 4H, CPC*H*CH), 8.09 (br, 4H, CHC*H*CC). $^{31}P\{^1H\}$ NMR (243 MHz, acetone-d_6): δ 12.2 (br s, $^1J_{Pt-P}$ = 2956 Hz), 14.9 (br s, $^1J_{Pt-P}$ = 3049 Hz), two small broad peaks were observed at δ 17.7 ppm (ca. 7%) and 23.8 ppm (ca. 12%). UV/vis (acetone): λ_{max} (ε in M^{-1} cm^{-1}) 329(18816), 373(12663) nm.

5, [Pd$_2$(dppf)$_2$(4,4′-SC$_{12}$H$_8$S)]$_2$(OTf)$_4$ (II). To a methanol solution of (5 mL) of **1b** (7.9 mg, 0.036 mmol) was added a dichloromethane solution (5 mL) of Pd(dppf)(OTf)$_2$ (69.5 mg, 0.072 mmol). The wine-red solution was stirred for 4 h. The solvent was evaporated in vacuuo; the red residue was washed with diethyl ether and extracted with acetone (3 × 5 mL). Diethyl ether (1 mL) was added to yield red crystal of the title complex (63.6 mg, 0.017 mmol, 95%; mp > 230 °C (dec)). Anal. Calcd for $C_{164}H_{128}F_{12}O_{12}P_8Pd_4S_8Fe_4$: C, 53.64; H, 3.51; S, 6.99. Found: C, 52.95; H, 3.29; S, 7.27%. ^1H NMR (500 MHz, acetone-d_6): δ 4.43 (s, 8H, H_{β}-ferr), 4.77 (s, 8H, H_{β}-ferr), 4.85 (s, 16H, H_{α}-ferr), 6.18 (br s, 8H, *o*-H, $C_{12}H_8$), 6.49 (d, $^3J_{HH}$ = 8.5 Hz,

DOI: 10.1021/acs.inorgchem.8b02726
Inorg. Chem. XXXX, XXX, XXX−XXX

Scheme 2. Syntheses of Palladium and Platinum Complexes with Arylenedithiols

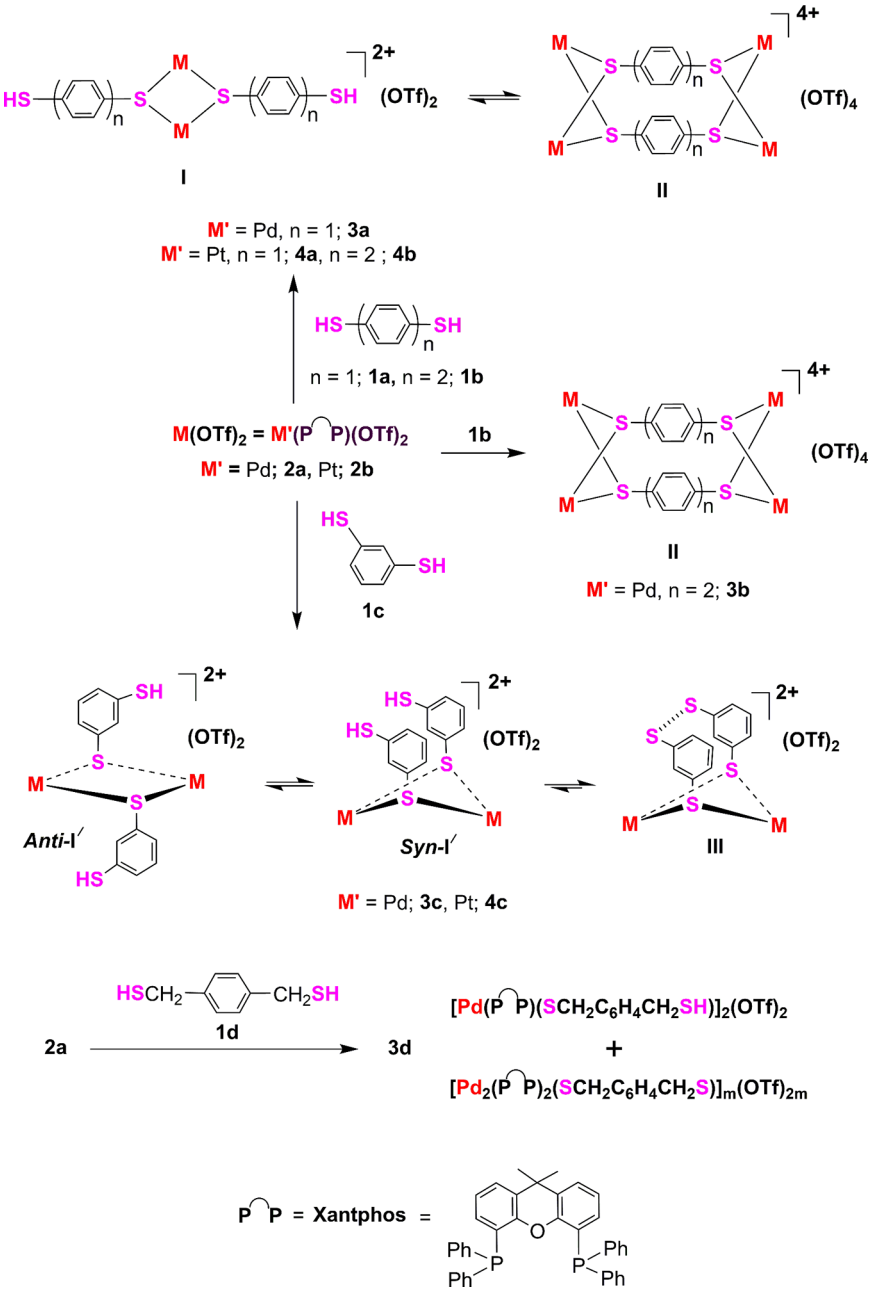

8H, *m*-H, $C_{12}H_8$), 7.62 (br s, 32H, *m*-H of Ph), 7.74 (br s, 16H, *p*-H of Ph), 7.80−7.99 (m, 32H, *o*-H of PPh_2). $^{31}P\{^1H\}$ NMR (243 MHz, acetone-d_6): δ 34.1 (s).

Suzuki−Miyaura Cross-Coupling Reaction. An oven-dried flask was charged with aryl halide (1 mmol), aryl boronic acid (1.3 mmol), palladium complex **3a** (0.1 mmol, equivalent to 0.4 mol % of Pd), methanol (3.0 mL), and aqueous K_2CO_3 (2 mmol, 1 mL) and placed on an oil bath at 70 °C under a nitrogen atmosphere; the reaction mixture was stirred until maximum conversion of aryl halide to product occurred. The reaction mixture was cooled to room temperature, was diluted with water (10 mL) and neutralized by dropwise addition of dilute HCl (aqueous). The mixture was extracted with hexane (3 × 15 mL), washed with water (2 × 10 mL) followed by brine solution (2 × 10 mL), and dried over anhydrous Na_2SO_4. The solvent of the extract was removed with rotary evaporator, and the resulting residue was analyzed by ^1H NMR spectroscopy.

Procedure for Catalyst Recycling. Similar to the above procedure, the reactants 4-bromoacetophenone (1.0 mmol), $PhB(OH)_2$ (1.3 mmol), and catalyst **3b** (0.4 mol %) were used. Keeping other reaction conditions as above, the mixture was stirred for 6 h and processed analogously. After the reaction, hexane (3 × 15 mL) was added to the product mixture resulting in the formation of two layers. The upper layer of hexane containing the product was removed to give 99% yield. Catalyst **3b**, contained in the lower aqueous layer, was then employed for another reaction; accordingly, a proportional amount of reactants were further added. After 6 h, the first reaction cycle resulted in 98% yield; in repeating the process, the second and third reaction cycles yielded 97 and 96% of the product.

Density Functional Calculations. Full geometry optimizations of all the Pd and Pt complexes are carried out using BP86 density functional. BP86 is a generalized gradient approximation functional that is formed by the combination of combines Becke's 1988 exchange functional with perdew's 1986 correlation functional.[29,30] Pseudo-Newton−Raphson based algorithm has been employed for

DOI: 10.1021/acs.inorgchem.8b02726
Inorg. Chem. XXXX, XXX, XXX−XXX

geometry search. Gaussian type double split valence basis functions, namely, 6-31G(d,p), are used for S, O, P, C, and H atoms, and 3-21G basis set for Pd is used for the calculations. SARC-ZORA basis set is used for Pt. The basis sets for Pt and Pd are obtained from Extensible Computational Environment Basis Set database (PNNL). The solvent water is modeled by employing conductor-like screening model (COSMO).[31] All electronic structure calculations are carried out applying the GAMESS suites of *ab initio* program systems on a LINUX cluster platform.[32] Visualizations of molecular geometry and orbitals are carried out by the MOLDEN and MOLEKEL program systems.[33,34]

RESULTS AND DISCUSSION

Syntheses and NMR Spectroscopy. The complexes $Pd(Xantphos)(OTf)_2$ (**2a**) and $Pt(Xantphos)(OTf)_2$ (**2b**) were isolated in 78 and 91% yield, respectively from the reaction of $Pd(Xantphos)Cl_2$ and $Pt(Xantphos)Cl_2$ with excess of AgOTf (OTf = CF_3SO_3). The crystalline Pd (yellow) and Pt (colorless) complexes are highly soluble in chlorinated solvents, methanol, acetone, etc., and were characterized by different analytical techniques. The two methyl groups showed a sharp singlet deshielded with respect to their chloride complexes. The $^{31}P\{^1H\}$ NMR spectrum showed one singlet with Pt satellites ($^1J_{Pt-P}$ = 4132 Hz) for **2b.** The X-ray structure of **2a** shows two coordinated water molecules with triflate as counteranions.

The reactions of bis triflate complexes **2a** and **2b** with arylene dithiols **1a** and **1b** in 2:1 ratio, immediately resulted in dark chocolate colored palladium complexes **3a** and **3b** and yellow colored platinum complexes **4a** and **4b** (Scheme 2). These new Xantphos-capped Pd(II) and Pt(II) complexes of dithiolate ligands were characterized by elemental analysis, NMR, UV/vis spectroscopy and mass spectrometry which are outlined in the Experimental Section. The $^{31}P\{^1H\}$ NMR spectrum of phenylene-1,4-dithiolate of palladium complex **3a** displayed two slightly broad peaks at δ 4.3 and 7.9 ppm. The analogous platinum complex **4a** also showed two comparatively sharp peaks at δ −8.5 and −1.5 ppm (Figure 1). The $^1J_{Pt-P}$ values of 3365 and 3494 Hz are significantly reduced relative to the $^1J_{Pt-P}$ value of **2b** due to the stronger trans influencing thiolate groups but are higher than those of the

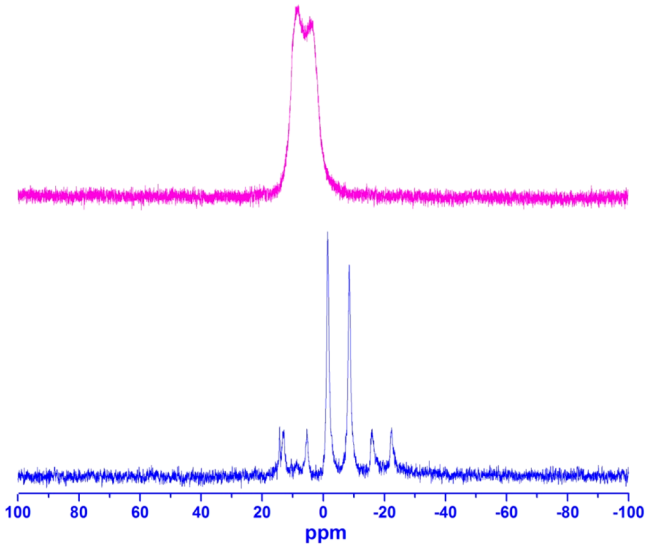

Figure 1. $^{31}P\{^1H\}$ NMR spectra (121 MHz, acetone-d_6) of **3a** (above) and **4a** (below).

PEt_3 analogue $[Pt_2(PEt_3)_4\{S(C_6H_4)_nS\}]_2(OTf)_4$ ($^1J_{Pt-P}$ = 2907−2911 Hz).[7] The present NMR data suggest the possibility of two types of complexes in solution. The single crystal X-ray diffraction analysis of **4a** confirmed the dinuclear structure $[Pt(Xantphos)(SC_6H_4SH)]_2(OTf)_2$ containing the "Pt_2S_2" bridge by two thiolates with two free thiols designated as **I** in Scheme 2.

As expected, complex **3b** showed a sharp peak at δ 9.1 ppm in $^{31}P\{^1H\}$ NMR spectrum (Figure S8). The ^1H NMR spectrum displayed two sharp singlets at δ 1.56 and 2.00 ppm for the methyl groups, two doublets for the ortho and meta hydrogens of the biphenylene group and other expected peaks in the aromatic region (Figure S6). The $^{31}P\{^1H\}$ NMR spectrum of the platinum complex **4b** showed a broad singlet with Pt satellites of $^1J_{Pt-P}$ about 3380 Hz (Figure S10). The pattern of ^1H and $^{13}C\{^1H\}$ NMR spectra of **4b** are similar to those of **3b**; however, the peaks are broadened, for example, the ortho and meta hydrogens or carbons of the biphenylene group showed two broad singlets (Figures S11−S13). The relative integration and elemental analysis indicates the composition $[M_2(SC_{12}H_8S)]_m(OTf)_{2m}$ for **3b** and **4b**. Single-crystal X-ray analyses of **4b** confirmed the tetranuclear structure $[Pt_2(Xantphos)_2(SC_{12}H_8S)]_2(OTf)_4$. It is noteworthy the analogous reactions of **1a** and **1b** with $M(OTf)_2$ (M = $[Pt(PEt_3)_2]^{2+}$ or $[Pd(dppe)]^{2+}$) resulted in the single products as tetranuclear complexes $[M_2\{S(C_6H_4)_nS\}]_2(OTf)_4$.[7] The possibility of two types of complexes in **3a** and **4a** at room temperature, as well as the broadening of the ^{31}P NMR peaks of **4b**, persuaded us to do low-temperature NMR experiments for the latter. The $^{31}P\{^1H\}$ NMR spectrum of **4b** was recorded in methanol-d_4 at three different temperatures (Figure 2). At room temperature, it

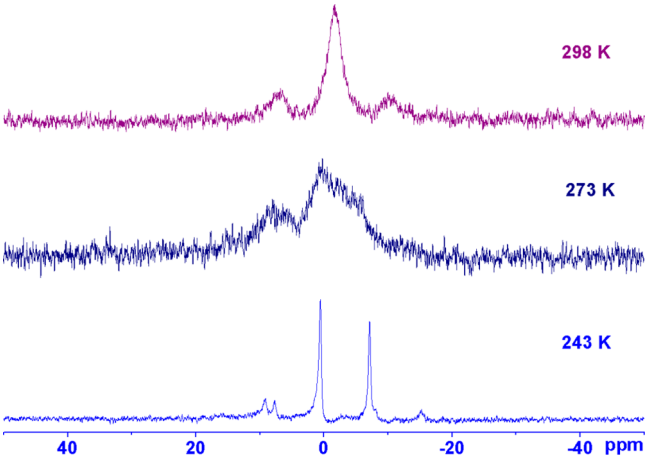

Figure 2. Variable-temperature $^{31}P\{^1H\}$ NMR spectra (202 MHz, CD_3OD) of **4b**.

seems the line broadening (full width at half-maximum, fwhm ∼ 531 Hz) is slightly more with approximate $^1J_{Pt-P}$ value of 3316 Hz as compared to the spectrum recorded in acetone-d_6 (fwhm ∼ 398 Hz). At 0 °C the main peak was extremely broadened and merged with the Pt satellites. After further lowering the temperature to −30 °C, it split into two sharp peaks at δ −7.1 and 0.5 ppm with Pt satellites; the respective $^1J_{Pt-P}$ values are 3228 and 3488 Hz. These spectral features have similarity with the ^{31}P NMR spectrum of **4a** which was recorded at room temperature. These results indicate that the two complexes, **I** and **II**, are in equilibrium which is fast at

DOI: 10.1021/acs.inorgchem.8b02726
Inorg. Chem. XXXX, XXX, XXX−XXX

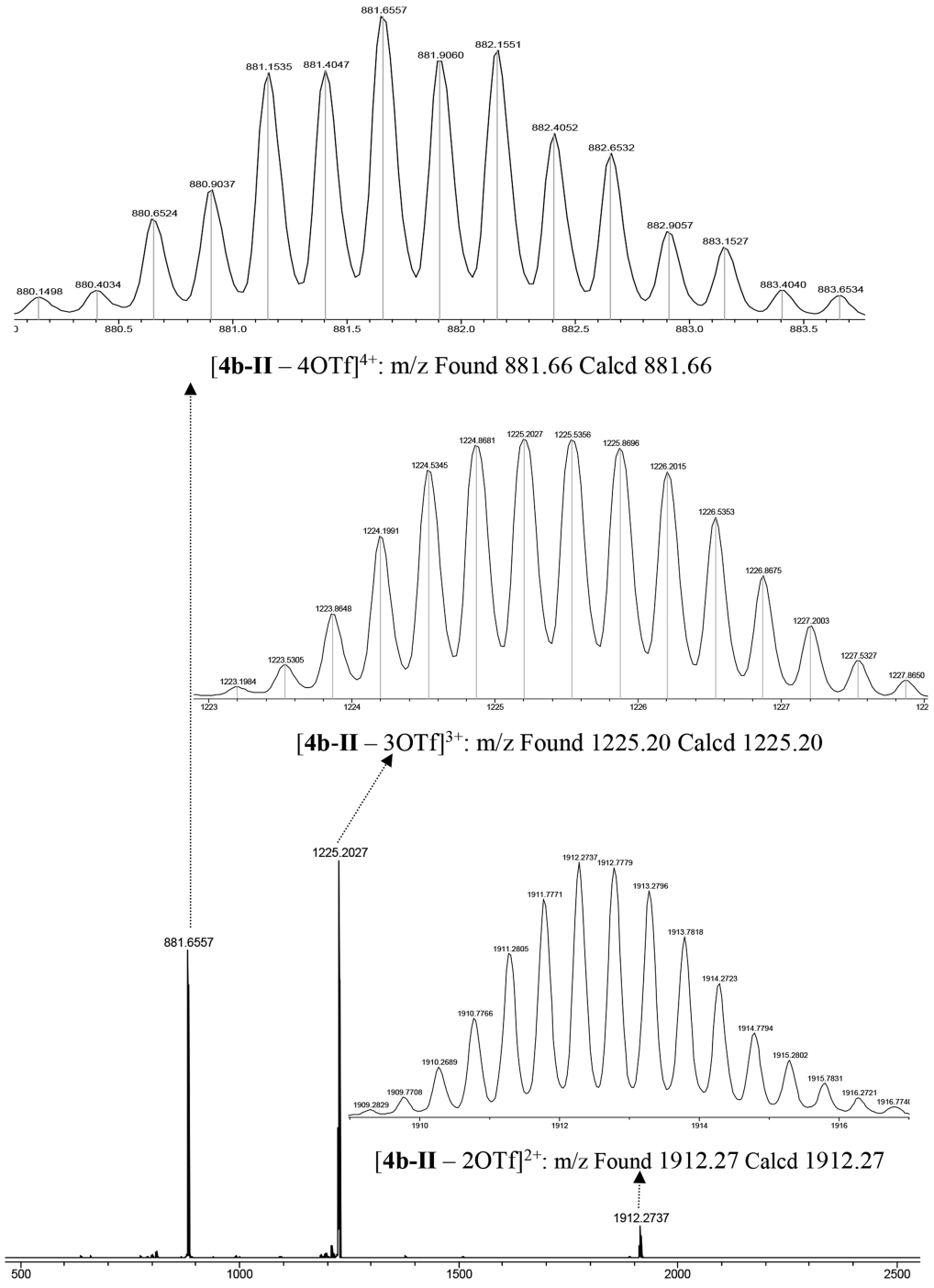

Figure 3. ESI mass-spectrum of **4b**. The insets show the experimentally obtained isotope patterns of the fragments. The found and calcd values are for the most abundant peak of the ion.

room temperature in the case of the biphenyl system. The sharp ^{31}P NMR peak for **3b** at room temperature may be attributed to the faster ligand-exchange processes in case of Pd complex as compared to that of Pt analogue. The wide bite angle and flexible behavior of the presently used ligand Xantphos, inducing a dynamic coordination environment around the crowded Pd(II) or Pt(II) centers, may be responsible for the fluxional nature of the resulted complexes.[35]

To confirm the other peak for methyl group, which is often merged with the solvent peak of acetone-d_6, the ^{1}H NMR spectra of **3a**, **3b**, and **4b** were recorded in methanol-d_4 (Figures S4, S7, and S12), which are outlined in the Experimental Section. Overall, the peaks are slightly more broadened in methanol-d_4 as compared to those in acetone-d_6. Moreover, the integration ratio of the peaks corresponding to the aromatic part of Xantphos group and dithiolate group are calculated as 1:1 for **3a** in methanol-d_4 and 1:1 for **4a** in acetone-d_6 which indicate the presence of **I** in solution. The thermal stability has been assessed by thermogravimetric (TG) analyses under argon atmosphere. The TG curve of **3b** shows the decomposition starts after 320 °C (Figure S32) which implies the solid compound is highly stable. However, palladium complexes **3a** and **3b** are found to be sensitive in chloroform. The ^{31}P{^{1}H} NMR spectrum of **3b** in $CDCl_3$

DOI: 10.1021/acs.inorgchem.8b02726
Inorg. Chem. XXXX, XXX, XXX−XXX

solution, when monitored for 3 days, showed an additional peak at δ 22.4 ppm with the peak at δ 8.0 ppm corresponding to **3b** in ~3:2 ratio; the former peak has been attributed to Pd(Xantphos)Cl_2.

Next, we sought to change the relative position of two thiol groups to see the effect of the ligand on the products and structures; accordingly, the same reactions were investigated with 1,3-benezenedithiol. The addition of **2a** and **1c** in 1:1 ratio initially gave a red colored product which shows three peaks at δ 15.9, 18.5, and 27.0 ppm in $^{31}P\{^1H\}$ NMR spectrum, the middle peak is broad whereas the later is highly sharp. In acetone-hexane mixture, this product yielded orange colored crystals, which displays a single resonance at δ 22.5 ppm, and the X-ray structure confirmed the dinuclear complex $[Pd_2(Xantphos)_2(SC_6H_4SSC_6H_4S)](OTf)_2$ (**3c-III**) containing a S−S bond between two thiolate ligands. The formation of these products was also monitored in an NMR tube. The mixing of **2a** and **1c** in acetone-d_6 within 1 h showed a peak at δ 15.9 ppm, which is attributed to the more likely *anti* conformer of **3c-I′** $[Pd(Xantphos)(SC_6H_4SH)]_2(OTf)_2$ (Scheme 2); however, after 1 day other prominent peaks appeared at δ 15.9, 18.5, 22.5, 27.0, and 47.0 ppm (Figures S15−S17). The broad peak at δ 18.5 ppm is assigned to *syn* conformer of **3c-I′** which is converted to **3c-III**, whereas the sharp peaks at δ 27.0 and 47.0 ppm are assigned to dioxide of Xantphos[36] and its Pd-ligated complex.

Similarly, the reaction of platinum complex **2b** and **1c** gives a yellow solid in solution which is transformed to a red product in a day. The $^{31}P\{^1H\}$ NMR spectrum of the yellow product exhibit two sharp doublets at δ 7.5 and 18.1 ppm with $^1J_{Pt-P}$ values 3057 and 2902 Hz, respectively (Figure S20). Although the structure could not be predicted, the elemental analysis suggest the composition of $[Pt(Xantphos)(SC_6H_4SH)]_n(OTf)_n$; the $^2J_{PP}$ value of about 24 Hz indicates two magnetically inequivalent ^{31}P nuclei. The $^{31}P\{^1H\}$ NMR spectrum of the red product (Figure S21) display mainly two broad singlets at δ 12.2 and 14.9 ppm with $^1J_{Pt-P}$ values 2956 and 3049 Hz, respectively, which have been assigned as *syn* and *anti* conformer of **4c-I′**, $[Pt(Xantphos)(SC_6H_4SH)]_2(OTf)_2$ (Scheme 2). The X-ray structure of the crystals found with the red product is established as the analogous structure of palladium complex $[Pt_2(Xantphos)_2(SC_6H_4SSC_6H_4S)](OTf)_2$ (**4c-III**). It may be noted in the case of **I** of **3a**, **3b**, and **4b** that a flat square-planar M'_2S_2 ring with two thiolate groups adopting an *anti* configuration,[37] has been assigned in solution that is confirmed by solid-state structure. The DFT calculations were also performed to check the feasibility of the analogous tetranuclear structure obtained from phenylene-1,4-dithiolate and biphenylene-1,4-dithiolate ligands. However, the calculations showed that the similar complex $[M'_2(Xantphos)_2(1,3\text{-}SC_6H_4S)]_2(OTf)_4$ (**II′**) with phenylene-1,3-dithiolate and the possibility of another neutral complex $[M'_2(Xantphos)_2(SC_6H_4S)_2]$ (**IV**) are inherently unstable, probably due to the overcrowding of ligands (Scheme S1). The reported platinum complex $[Pt_2(terpyridine)_2(1,3\text{-}SC_6H_4S)](PF_6)_2$ exist as linear dimeric complex.[38]

Another bridging ligand 1,4-benzenedimethanethiol was also taken up to check the above results, and to compare the catalytic activity. The $^{31}P\{^1H\}$ NMR spectrum of the prepared palladium complex **3d**, shows two broad peaks at δ 10.8 and 12.9 ppm, which suggest also two types of complexes (Figure S22). The dppe analogue has been reported as octanuclear structure with Pd:dithiolate ratio is 2:1.[7] In the present case, by analogy, two types of complexes $[Pd(Xantphos)(SCH_2C_6H_4CH_2SH)]_2(OTf)_2$ and $[Pd_2(Xantphos)_2(SCH_2C_6H_4CH_2S)]_m(OTf)_{2m}$ have been tentatively assigned which was not proceeded further (Scheme 2). Palladium complex **5** of bisphosphine dppf, containing a wide bite angle (106°) but smaller than that of Xantphos, has been prepared with **1b** as another catalyst for comparative study. The NMR spectrum and single crystal structure of **5** confirmed the tetranuclear structure $[Pd_2(dppf)_2(SC_{12}H_8S)]_2(OTf)_4$ of type **II**, both in solution and solid state.

Mass Spectrometry. The mass spectra of the complexes were obtained by soft ionization ESI technique. The ESI mass spectra clearly showed the molecular ion peaks minus the counterions and confirm the formation of the complexes (Figures 3 and S25−S27). The fragmented ions are observed with +1 to +4 charge states, the peaks are isotopically resolved which agree well with their theoretical distributions (Tables S3 and S4). For **3a**, the relevant peaks were observed at m/z 1165.1, 825.1, and 754.1 corresponding to $[\mathbf{3a\text{-}II} + H - (3OTf + Pd(Xantphos) + 2C_6H_4)]^{2+}$, $[\mathbf{3a\text{-}I} - (2OTf + Pd(Xantphos)(SC_6H_4SH))]^+$, and $[\mathbf{3a\text{-}II} - (4OTf + Pd_2(Xantphos)_2(SC_6H_4S))]^{2+}$. A similar mass spectrum was observed for the analogous biphenylene dithiolate complex of palladium **3b**; the peaks at m/z 901.1 and 816.6 have been attributed to $[\mathbf{3b\text{-}II} - (4OTf + Pd_2(Xantphos)_2)]^{2+}$ and $[Pd_2(Xantphos)_2S(OTf) + 2CH_3CN + 2H]^{2+}$ suggesting the tetranuclear structure $[Pd_2(Xantphos)_2(SC_{12}H_8S)]_2(OTf)_4$. However, no peak corresponding to binuclear structure was detected in case of **3b**.

The mass analyses of platinum complexes **4a** and **4b** show lesser fragmentation than palladium complexes. The prominent peaks were observed for **4a** at m/z 1299.7 ($[\mathbf{4a\text{-}II} - (4OTf + Pt(Xantphos))]^{2+}$), 1173.8 ($[\mathbf{4a\text{-}II} - 3OTf]^{3+}$), and 914.1 ($[\mathbf{4a\text{-}I} - (2OTf + Pt(Xantphos)(SC_6H_4SH))]^+$). Similarly, for analogous dithiolate complex **4b**, the peaks at m/z 1911.3 ($[\mathbf{4b\text{-}II} - 2OTf]^{2+}$), 1224.5 ($[\mathbf{4b\text{-}II} - 3OTf]^{3+}$), and 881.2 ($[\mathbf{4b\text{-}II} - 4OTf]^{4+}$) confirm the formation of tetranuclear complex **II**. The mass analysis of both **3a** and **4a** strongly support the presence of **II** as another complex by a large number of fragmented ions, as indicated by NMR spectroscopic data. The other complex, **I**, is confirmed by the X-ray structure of **4a**.

UV/Vis Absorption Spectra. The Pd complexes are dark maroon colored, and the Pt complexes are yellow colored crystalline solids. The absorption spectrum in acetone solution show a broad but strong band in the visible region, which is responsible for the color of the complexes (Figure S29−S30). Palladium complexes **3a**, **3b**, and **3c** display a long wavelength band at 503, 518, and 461 nm, respectively, whereas analogous platinum complexes **4a**, **4b**, and **4c** display the absorption in higher energies at about 447, 411, and 373 nm. It is to be noted that the similar band is absent in the case of starting precursors **2a** or **2b**. This long wavelength band has been assigned to S and phenyl ring orbitals based HOMO to phosphine and metal orbital based LUMO charge transfer transition in the case of analogous complexes of dppe/Pd and PEt_3/Pt systems,[7] which has been analyzed by DFT calculations (see below). However, the bands of the present Xantphos complexes are bathochromically shifted in comparison to the dppe or PEt_3 analogues. The complexes $[Pd_2(dppe)_2(SC_{12}H_8S)]_2(OTf)_4$ and $[Pt_2(PEt_3)_4(SC_{12}H_8S)]_2(OTf)_4$, similar to **3b** and **4b**, showed absorption maxima at 447 and 364 nm, respectively.[7] The molar extinction

DOI: 10.1021/acs.inorgchem.8b02726
Inorg. Chem. XXXX, XXX, XXX−XXX

coefficient value of the order $\sim 10^4$ M^{-1} cm^{-1} suggest a symmetry allowed transition.

Crystal Structures. Molecular structures of $[Pt(Xantphos)(SC_6H_4SH)]_2(OTf)_2$ (**4a-I**), $[Pt_2(Xantphos)_2(SC_{12}H_8S)]_2(OTf)_4$ (**4b-II**), $[Pd_2(Xantphos)_2(SC_6H_4SSC_6H_4S)](OTf)_2$ (**3c-III**), $[Pt_2(Xantphos)_2(SC_6H_4SSC_6H_4S)](OTf)_2$ (**4c-III**), and $[Pd_2(dppf)_2(SC_{12}H_8S)]_2(OTf)_4$ (**5**) were established by single crystal X-ray analyses. All structures are cationic, as the triflate ions are placed at large, nonbonding distance from palladium or platinum centers. In case of **4a-I**, **4b-II**, **4c-III** and **5** the triflate ions were found highly disordered and was initially modeled using partial occupancies with multiple conformations. However, no satisfactory model could be obtained, therefore the triflate ions were removed from the model and the refinement was carried out using solvent mask utility as implemented in Olex2.[39] ORTEP drawing with atomic numbering schemes are shown in Figures 4−7 and S33 while selected interatomic parameters are given in Table 1.

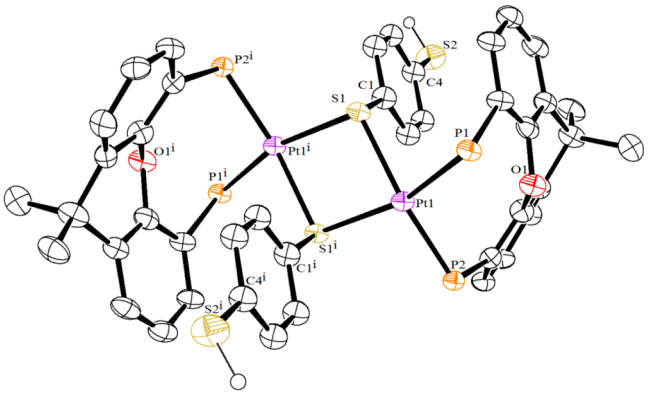

Figure 4. Single-crystal X-ray structure of $[Pt(Xantphos)(SC_6H_4SH)]_2(OTf)_2$ (**4a-I**) ellipsoids drawn at 25% probability. The triflate ions were masked, the phenyl groups of Xantphos and hydrogen atoms except for thiol groups are omitted for clarity.

The cationic part of complex **4a-I** is a centro-symmetric binuclear molecule, in which two Pt atoms are held together by bridging thiolato group of the ligand with the free thiol groups adopting an *anti* configuration. The geometry around Pt(II) is

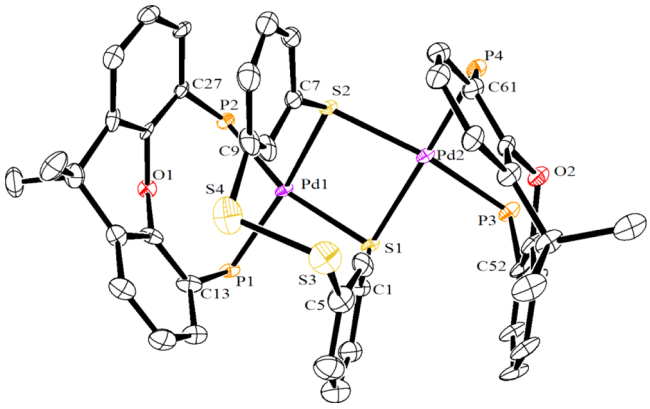

Figure 6. Single-crystal X-ray structure of $[Pd_2(Xantphos)_2(SC_6H_4SSC_6H_4S)](OTf)_2$ (**3c-III**) ellipsoids drawn at 25% probability. The triflate ions, the phenyl groups of Xantphos and hydrogen atoms are omitted for clarity.

distorted square planar whereas the $[Pt_2(\mu\text{-}SAr)_2]$ core is planar rhombus shaped. The two phosphorus atoms stay above and below the Pt_2S_2 plane by 0.6 and 0.8 Å. The backbone of the xanthene moiety is as usual nonplanar. One side of the coordination plane of Pt center is crowded by the three phenyl rings of both the ligands. The $\pi\cdots\pi$ stacking distance between the phenyl ring of thiolate group and the nearest phenyl ring of the xanthene group is 3.7 Å. The intermolecular S···S and S···H distances found as 3.54 and 4.14 Å.

The tetranuclear structures of $[M'_2(P^{\cap}P)_2(SC_{12}H_8S)]_2(OTf)_4$ ($M'/P^{\cap}P$ = Pt/Xantphos, **4b-II**; Pd/dppf, **5**) resemble the structure of Pd/dppe analogue.[7] The macrocyclic structures consist of two 4,4′-biphenylenedithiolate ligands which bridge two "$M'_2(P^{\cap}P)_2$" units at head and tail positions. The resulting four-membered nonplanar "M'_2S_2" rings at both the ends capped by two Xantphos or dppf ligands look over crowded compared to the Pd/dppe analogue. The dihedral angle between two S−Pt−S planes is 48.1° in **4b-II**, whereas it is 44.1° between S−Pd−S planes in **5**. The length of the rectangle as earlier defined by edge-to-edge S···S distance is 10.6 Å, and the height defined by the S···S distance in a same M'_2S_2 unit is 3.1 Å in both the structures. The $\pi\cdots\pi$ stacking distance between the two opposite centroids of benzene rings

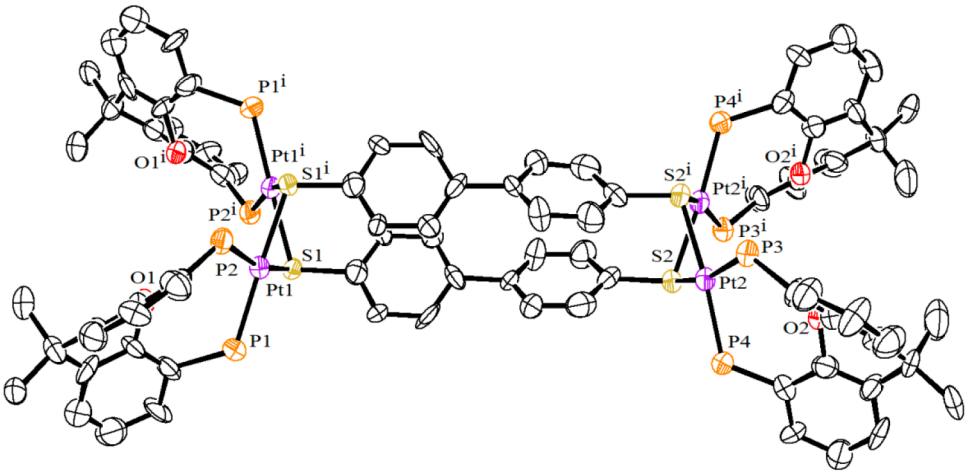

Figure 5. Single-crystal X-ray structure of $[Pt_2(Xantphos)_2(SC_{12}H_8S)]_2(OTf)_4$ (**4b-II**) ellipsoids drawn at 25% probability. The triflate ions were masked, the phenyl groups of Xantphos and hydrogen atoms are omitted for clarity.

DOI: 10.1021/acs.inorgchem.8b02726
Inorg. Chem. XXXX, XXX, XXX−XXX

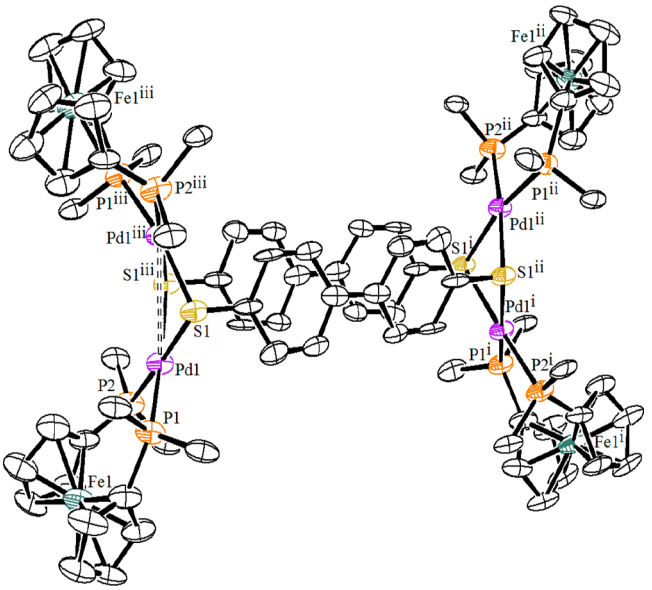

Figure 7. Single-crystal X-ray structure of $[Pd_2(dppf)_2(SC_{12}H_8S)]_2(OTf)_4$ (**5**) ellipsoids drawn at 25% probability. The triflate ions were masked, the phenyl groups of dppf and hydrogen atoms are omitted for clarity.

of dithiolate ligand are ∼3.5 and 3.4 Å, respectively, for platinum and palladium structures. Similarly, for another $\pi\cdots\pi$ stacking the closest distance between one phenyl ring attached to P atom and phenyl ring of Xanthene backbone is 4.0 Å in **4b-II**.

The dinuclear structures of **3c-III** and **4c-III** can be envisioned as the modified form of the *syn* conformer of **4a-I** after bonding between two free SH groups of two different ligands containing one thiolate and another thiol form positioned at 1,3-position in the benzene ring. It forms a rigid but unique unit "$PtSC_6H_4SSC_6H_4SPt$" having a S−S bond. It is noteworthy that the similar reactions of three dithiols **1a−1c** with $\{[(PPh_3P)Au]_3O\}^+BF_4^-$ resulted only in Au(I) thiolates without any such S−S bond in the complexes.[40] This is probably due to the square planar geometry of M′(II) in addition to the bridging mode of thiolate ligand and tetrahedral geometry around "S" atom favors the S−S bonding in a suitable position. The S−S bond distance of 2.07 Å in both the structures match well with S−S bond distances in Pt complexes such as in $[PtS_4(dppe)]$ (avg 2.04 Å),[41] $[Pt_2(4,4'\text{-}py_2S_2)_2(PEt_3)_2](NO_3)_2$ (2.03 Å).[9] The $\pi\cdots\pi$ stacking distance found between the phenyl ring of thiolate group and the nearest phenyl ring of the xanthene backbone is 3.6 Å. Unlike in **4a-I**, the M'_2S_2 rings are nonplanar; the calculated dihedral angles for **3c-III** and **4c-III** are 23.4 and 21.6°. However, these hinge distortions are comparatively less than that in **4b-II** or **5**.

A slight variation in Pt−S bond distances was noticed in all the three structures: 2.37−2.39 Å for for **4a-I**, 2.36−2.37 Å for **4b-II**, and 2.37−2.39 Å for **4c-III**. These distances match well with the Pt−S bond distances in analogous complex $[Pt_2(\mu\text{-}o\text{-}SC_6H_4(CF_3))_2(dppe)_2](OTf)_2$ (2.38 Å)[42] but are longer than those in in $[Pt_2(dppf)_2(C_8H_8NS)](BF_4)$ (2.34 Å)[43] and $[Pt_2(terpyridine)_2(1,3\text{-}SC_6H_4S)]_2(PF_6)_2$ (2.31 Å).[38] The bite angles (101−102°) for **4a-I** and **4b-II** agree well with those of complexes $[Pt(Xantphos)Cl_2]$[44] (101°) and $[Pt_3(Xantphos)_2\{(SeCH_2)_2C(CH_2OH)_2\}]Cl_2]$[44] (101°) but are smaller than that of the allyl complex $[Pt(\eta^3\text{-allyl})(Xantphos)](OTf)$ (107°),[45] whereas the bite angles 98−99° for **3c-III** are shorter than the usual values for a wide bite angle (>101°) in Xantphos complexes. Although the exact reason is not clear, the P···P distances (3.50 Å) are found to be shorter in **4c-III** in comparison to those in **4a-I** (3.56 Å) and **4b-II**(3.59 Å). In the case of Pd(0) complexes, a correlation has been noticed among P···P separation, Pd−P distances, and P−Pd−P bite angles.[46] The average Pt−P bond distances of about 2.30−2.32 Å for the three complexes match well with the reported Pt−P bond distances of Xantphos complexes Pt(II).[44,45]

The structure of $[Pd(Xantphos)(OH_2)_2](OTf)_2\cdot(H_2O)_{1.5}(CH_2Cl_2)_{0.5}$ $\{$**2a**$\cdot(H_2O)_{3.5}(CH_2Cl_2)_{0.5}\}$ shows two water molecules coordinated to palladium center, whereas the triflate anions remain separated in the lattice with electrostatic interactions with complex cations. The solvent molecules water and dichloromethane were also found in the lattice (Figure S34). The coordinated water molecules and O-atoms of triflate anions are involved in hydrogen bonding. The Pd−P bond length (∼2.24 Å) matches well with the Pd−P distances in complexes of large bite angle phosphines

Table 1. Selected Interatomic Distances [Å] and Angles [°] of 4a-I, 4b-II, 3c-III·$(CH_3COCH_3)_2$, 4c-III, and 5

	4a-I	4b-II	4c-III	3c-III	5
		M = Pt		M = Pd	
M1−S1	2.3871(17)	2.364(2)	2.371(3)	2.414(3)	2.3660(19)
M1−S1[a]/S2	2.3720(16)	2.368(2)	2.395(3)	2.371(3)	2.384(2)
M2−S2		2.355(2)	2.379(3)	2.389(3)	
M2−S2[a]/S1		2.366(3)	2.382(3)	2.382(3)	
M1−P1	2.3005(17)	2.318(3)	2.294(3)	2.324(3)	2.340(2)
M1−P2	2.3044(18)	2.322(2)	2.293(3)	2.309(4)	2.326(2)
M2−P3		2.325(3)	2.313(3)	2.315(4)	
M2−P4		2.311(3)	2.291(3)	2.360(4)	
S1−M1−S1[a]/S2	81.91(6)	82.34(9)	83.00(10)	84.55(11)	83.14(8)
S1−M1−P1	85.06(6)	93.65(9)	85.56(11)	95.79(12)	86.66(8)
S1−M1−P2	158.47(7)	163.42(10)	164.21(12)	163.38(12)	173.78(8)
P1−M1−P2	101.22(7)	101.00(10)	97.93(11)	98.04(13)	99.54(9)
S2−M2−S2[a]/S1		82.08(10)	83.12(10)	84.87(11)	
P3−M2−P4		101.90(10)	99.07(11)	98.68(13)	

[a]Symmetry related atom.

DOI: 10.1021/acs.inorgchem.8b02726
Inorg. Chem. XXXX, XXX, XXX−XXX

Table 2. Energy Parameters of Complexes Calculated Applying BP86 DFT Functional

	Pd complex				Pt complex			
	3a-I	**3a-II**	**3b-II**	**3c-III**	**4a-I**	**4a-II**	**4b-II**	**4c-III**
HOMO−LUMO gap (eV)	1.39	1.42	1.43	1.73	1.65	1.68	1.68	2.04
stability (kcal/mol)	−435	−870	−872	−1199	−538	−1068	−1069	−1298

Table 3. Reaction between Aryl Halide and Aryl Boronic Acid[a]

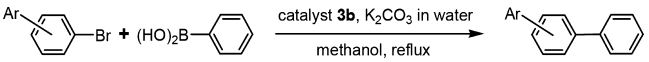

entry	ArBr	complex	time (h)	mol % of "Pd"	yield (%)[b]	TON	TOF (h^{-1})
1	4-$CH_3C_6H_4Br$	$PdCl_2$[c]	6	0.4	12	30	5
2	4-$CH_3C_6H_4Br$	$Pd(OAc)_2$	6	0.4	54	135	23
3	4-$CH_3C_6H_4Br$	$PdCl_2(PPh_3)_2$[d]	6	0.4	70	175	29
4	4-$CH_3C_6H_4Br$	$PdCl_2$(Xantphos)[d]	6	0.4	25	63	11
5	4-$CH_3C_6H_4Br$	**3a**	6	0.4	96	240	40
6	4-$CH_3C_6H_4Br$	**3a**	10	0.04	90	2250	225
7	4-$CH_3C_6H_4Br$	**3b**	10	0.04	83	2075	208
8	4-$CH_3C_6H_4Br$	**3c**	10	0.04	70	1750	175
9	4-$CH_3C_6H_4Br$	**3d**	10	0.04	67	1675	168
10	4-$CH_3C_6H_4Br$	**3a**	10	0.004	78	19500	1950
11	4-$CH_3C_6H_4Br$	**3b**	10	0.004	70	17500	1750
12	2-$OHCC_6H_4Br$	**3a**	10	0.04	92	2300	230
13	4-$CH_3COOC_6H_4Br$	**3a**	6	0.4	97	243	41
14	4-$O_2NC_6H_4Br$	**3a**	6	0.4	98	245	41
15	4-FC_6H_4Br	**3a**	6	0.4	80	200	33
16	4-CNC_6H_4Br	**3b**	10	0.04	94	2350	235
17	4-CNC_6H_4Br	**3d**	10	0.04	68	1700	170
18	4-$OHCC_6H_4Br$	**3a**	10	0.04	95	2375	238
19	4-$OHCC_6H_4Br$	**3c**	10	0.04	79	1975	198
20	4-$OHCC_6H_4Br$	**3d**	10	0.04	70	1750	175
21	4-$CH_3OC_6H_4Br$	**3a**	6	0.4	44	110	18
22	4-$CH_3OC_6H_4Br$	**3a**	6	0.4	98[e]	245	41
23	4-$OHCC_6H_4Cl$	**3b**	16	2	29[f]	15	1
24	4-$OHCC_6H_4Cl$	**3a**	28	2	47[g]	24	0.8
25	1-$C_{10}H_7Br$	**3a**	6	0.4	94	235	39
26	2-SC_4H_3Br	**3a**	6	0.4	80	200	33
27	2-SC_4H_3Br	**3b**	6	0.4	78	195	33
28	2-SC_4H_3Br	**3d**	6	0.4	68	170	28
29	4-NC_9H_6Br	**3a**	6	0.4	86	215	36

[a]Conditions: Aryl halide (1.0 mmol), phenyl boronic acid (1.3 mmol), K_2CO_3 (2 mmol) in H_2O, methanol (3 mL). [b]Determined by ^1H NMR spectroscopy. [c]CH_3CN/MeOH. [d]$CHCl_3$/MeOH. [e]TBAB (1 mmol) used. [f]TBAB (5 mmol) used. [g]TBAB (3 mmol) used.

$[Pd(P^{\cap}P)(OH_2)_2](OTf)_2$ ($P^{\cap}P$: dppf (2.26 Å),[47] dppn ((diphenylphosphino)binaphthyl, 2.24 Å)[48] (Table S5). The bite angle ∼101° agrees with the bite angles for other complexes such as [Pd(η^3-benzyl)(Xantphos)](OTf)[25] (107°) and [Pd(η^3-allyl)(Xantphos)](OTf)[9] (107°).

DFT Calculations. Geometry optimizations of the structures were carried out by applying BP86 functional with mixed atomic basis functions for the metal and other atoms. This functional performed well for the Pd/Pt based complexes.[7] The final optimized structures of Pd and Pt complexes resemble the available X-ray structures; the selected bond distances and angles are summarized in Table S6. The calculated distances of Pt−S and Pt−P bonds are ∼0.13 Å longer than the experimental data of the complexes **4a-I**, **4b-II**, **4c-III**, and **3c-III**. The deviation in bond distance may be attributed to the unavailability of larger basis set for the metal. The calculated S−Pt−S and P−Pt−P angles match very closely with the X-ray data.

The calculations of the frontier orbitals, namely, the highest occupied molecular orbitals (HOMO) and the lowest unoccupied molecular orbitals (LUMO) of all the complexes are also carried out and are plotted in Figures S35 and S36. It is observed that the HOMO is composed of orbitals mainly from phenylene group of the aryl dithiolate ligands with some additional contributions from S 3p, P 3p, and Pd 4d or Pt 5d orbitals (Table S7), whereas the LUMO is formed as more mixed orbitals spread over the system with significant contributions from metal and phenylene orbitals. Thus, the long wavelength band is attributed to the electronic transition, from phenylene based HOMO to a LUMO, composed of mixed orbitals. The calculated values of HOMO−LUMO gap for **I** and **II** are close to each other, i.e., 1.39−1.42 eV for Pd complexes and 1.65−1.68 eV for Pt complexes (Table 2). Similarly, changing from phenylene to biphenylene system there is hardly any change of energy, such as 1.42 and 1.43 eV for **3a-II** and **3b-II** and 1.68 eV for **4a-II** and **4b-II**. This is in agreement with the slight change in the low energy absorption

DOI: 10.1021/acs.inorgchem.8b02726
Inorg. Chem. XXXX, XXX, XXX−XXX

Table 4. Effect of Catalyst Loading on Suzuki Reaction[a]

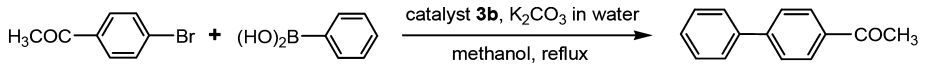

entry	mol % of "Pd"	time (h)	% yield[b]	TON	TOF (h^{-1})
1	0.1	6	97	970	162
2	0.01	6	95	9500	1583
3	0.001	6	91	91000	15167
4	0.001	10	94	94000	9400
5	0.0001	10	92	920000	92000
6	0.00001	10	76	7600000	760000
7	0.000001	10	51	51000000	5100000

[a]Conditions: 4-Bromoacetophenone (1.0 mmol), phenyl boronic acid (1.3 mmol), K_2CO_3 (2 mmol) in H_2O, methanol (3 mL). [b]Determined by ^1H NMR spectroscopy.

band, i.e., 503 and 518 nm for **3a** and **3b**, respectively. However, replacing the metal center Pd by Pt, the HOMO−LUMO gap increases by 0.25 eV as calculated on going from complex **3a** to **4a** or from **3b** to **4b**. This change qualitatively agrees with the hypsochromic shift of the long wavelength band, as the difference in energy of 0.31 eV of the experimental absorption maximum calculated for **3a** (503 nm, ≈2.46 eV) and **4a** (447 nm, ≈2.77 eV). It is clear from Table S7 that there is almost no change in energy of HOMO for **3a-II** and **4a-II**; however, a slight destabilization is observed when their LUMO energy levels are considered. The LUMO, composed of large contribution from metal orbital, which interact with S and P orbitals. In the case of Pt complexes, the 5d orbitals of higher energy and larger size can strongly interact, hence more destabilization, as compared to 4d orbitals in Pd complexes. The HOMO−LUMO gap further widen up to ≈0.3 eV in the complexes of 1,3-phenylenedithiolate. The absorption maxima, 461 nm for **3c** and 373 nm for **4c**, are hypsochromically shifted, as compared to the absorption in complexes of 1,4-phenylenedithiolate (**3a** or **4a**) and 4,4′-biphenylenedithiolate (**3b** or **4b**).

Interestingly, the relative stability significantly differs from one structure to another or Pd to Pt complexes. The stability as well as the HOMO−LUMO energy gap follows the order **III** > **II** > **I**, irrespective of metal center. Macrocyclic tetranuclear complexes **II** are more stable than the "M'_2S_2" bridged dinuclear complexes **I**, at ca. −435 kcal/mol for Pd complex **3a** and −530 kcal/mol for Pt complex **4a**, whereas **II** of phenylenedithiolate and biphenylenedithiolate systems are almost equally stable in the cases of both Pd (**3a**, **3b**) and Pt (**4a**, **4b**) complexes (Table 2). An extra stability gained by the comparatively rigid structures by forming S−S bond in the complexes **3c-III** (−1199 kcal/mol) and **4c-III**(−1298 kcal/mol). Considering **I** and **I′** have comparable stability, the large difference in stability between **I′** and **III**, facilitate their transformation via the *anti*-to-*syn* conversion of **I′**, presuming the *syn* configuration is slightly less preferable than *anti* configuration. The varied stability of **I**, **II**, and **III** can influence the catalytic activity of the Pd complexes.

Suzuki Cross-Coupling Reactions. The catalytic applications of the palladium complexes were investigated in the Suzuki cross-coupling reactions of aromatic substrates. There are only few reports, employing Pd(II) thiolates as catalysts in Suzuki or C−C cross-coupling reactions, and to our knowledge, no reports are available using the Pd complexes of Xantphos and thiolate ligands. The catalytic activities of Pd complexes **3a**, **3b**, **3c**, and **3d** were evaluated in the coupling reactions of phenylboronic acid and aryl halides. The reactions of the unactivated 4-bromotoluene with phenylboronic acid were chosen as the model reaction which was initially optimized with respect to solvent, base, and temperature. As the present Pd complexes are poorly soluble in dioxane which is also carcinogenic in nature,[49] the other solvents such as DMA, DMF, and methanol were used for screening. Surprisingly, the refluxing condition in methanol at 78 °C gave better results than in DMA and DMF at higher temperatures, 95 and 104 °C, respectively, which is attributed to methanol being a more efficient reductant, as compared to DMA or DMF. There might be better coordination in case of methanol to the palladium center in the transition state.[50] When using methanol as solvent in Suzuki reactions, activities increased dramatically for palladacycles containing thioether group.[51] The inorganic bases K_2CO_3, Cs_2CO_3, KOH, and Na_2CO_3 afforded higher yields than the organic bases Bu_4NOH, Et_3N. K_2CO_3 was chosen as base for the investigations. As expected, the yield of the product increased with the temperature. The variation of time showed 93% of the coupling product within 2 h of reaction time, which leveled off at 6 h. Under the optimized reaction condition, the traditional Pd salts showed lower catalytic activity (Table 3, entries 1−4) in comparison with those of the present complexes.

The effect of varying the arylbromides was investigated under the optimized reaction condition with phenylboronic acid, and results are presented in Table 3. The activated (entries 12−20) and nonactivated (entries 5−7) arylbromides resulted in very good quantitative yields (80−98%) of the biaryls by using 0.4−0.04 mol % Pd. A variety of functional groups such as aldehyde, acetyl, nitro, cyano, and so on are tolerated. The deactivated aryl bromide, 4-bromoanisole gave a somewhat lower conversion; however, with the addition of 1 equiv of TBAB, the yield became excellent (entries 21−22). We also investigated the electronically activated aryl chloride; the best yield 47% was obtained for the coupling of 4-chlorobenzaldehyde, in the presence of 3 mol % TBAB (entry 24). Moreover, the reaction with heteroaryl bromides and naphthyl bromide also led to the formation of the desired products in moderate to excellent yields (68−94%, entries 25−29).

The performance of low catalyst loading was tested in the coupling reactions of both activated and nonactivated arylbromides. For 4-bromoacetophenone, although the yields are gradually decreased from 97 to 51%, with lowering of concentration of catalyst **3b** from 0.1 to 0.000001 mol % of Pd, the resulted turnover numbers (TON) become very high up to 5×10^7 (Table 4). A similar trend was found in the case of 4-bromotoluene: The yields 78 and 70% were obtained when at

DOI: 10.1021/acs.inorgchem.8b02726
Inorg. Chem. XXXX, XXX, XXX−XXX

Table 5. Reusability Experiment[a]

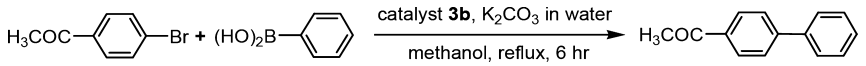

cycle	0	1	2	3	4	5	6	7	8
% yield[b]	99	98	97	96	94	93	91	89	85

[a]Conditions: 4-Bromoacetophenone (1.0 mmol), phenyl boronic acid (1.3 mmol), K_2CO_3 (2 mmol) in H_2O, methanol (3 mL), 0.4 mol % of Pd used. [b]Determined by ^1H NMR spectroscopy.

loadings of Pd of **3a** and **3b** were decreased to 0.004 mol %, and the corresponding TONs are 2×10^4, indicating both the catalysts are active (Table 3). Moreover, the feasibility of the repeated use of the Pd catalyst was examined. In Table 5, the results of the coupling reaction of 4-bromoacetophenone and phenylboronic acid by **3b** for eight consecutive cycles are summarized. After completion of each round, hexane was added to extract the organic part having the product; then, to the remaining aqueous layer containing the catalyst, the required amounts of reactants were freshly added for the next round of reaction. The yields were remained very high, from 99 to 85%, even after 8 successive cycles, which suggests the catalyst is still very active.

All the Pd complexes show good catalytic activities under mild conditions as revealed in Table 3. However, the fine comparison of the yields (entries 6–9; 18–20; and 26–28) shows that the catalytic activities follow the order **3a** > **3b** > **3c** > **3d**. The trend may be explained based on the relative stability of the structures with the order **III** > **II** > **I**. The DFT calculations show the reasonable differences among them as calculated between **3b-II** and **3a-I** is 437 kcal/mol and for **3c-III** and **3b-II** is 327 kcal/mol (Table 2). The proportions of **I** and **II** in phenylene-1,4-dithiolate complex **3a** are almost equal in solution as indicated by ^{31}P NMR spectrum, whereas in the case of 4,4′-biphenyldithiolate complex **3b**, only complex **II** exclusively exists in solution. Thus, the contribution of comparatively less stable **I** makes complex **3a** more catalytically active or vice versa for **3c**. A similar phenomena was observed in the case of dppe analogue.[7] The catalytic activities of the present complexes are comparable with the reported Pd supramolecular and macrocyclic complexes under mild conditions and low loading (Table S8).

To evaluate the effect of varied bite angles of bis-phosphine on the catalytic activity, dppe and dppf were chosen for comparison with Xantphos. The ligand 4,4′-biphenylenedithiolate was selected as it can form tetranuclear complex-$[Pd_2(P^{\frown}P)_2(SC_{12}H_8S)]_2(OTf)_4$ as single product in solution. In the present reaction condition, i.e., reflux in methanol, among the complexes of three phosphines, Xantphos derivative gave the highest yield (Table S9). The Pd complexes of Xantphos, dppf, and dppe, encompassing bite angles of 104.6, 99.6, and 84.7°, respectively, yielded 70, 51, and 42% of product using 0.004 mol % of Pd as catalyst. The high activity of Xantphos complex points to its flexible coordination behavior, which is absent in dppe and dppf, apart from the large bite angle.[35]

Though it is difficult to identify the active catalyst, preliminary investigations were carried out to learn the nature of the Pd complex after the catalysis reaction. The UV–vis spectrum of the compound separated after the zero cycle of catalysis reaction of **3b** showed a long wavelength absorption band at 408 nm (Figure S31), whereas a similar band observed at 518 nm for **3b**. The ESI mass spectrum of the same brown colored compound displayed the prominent peaks at m/z 1395.2 and 1551.2 corresponding to $[Pd(Xantphos)(SC_{12}H_8S)(SC_6H_4)(OTf)_2 + 4CH_3CN - C_6H_5]^+$ and $[Pd_2(Xantphos)_2(S(C_6H_4)S) + CH_3CN + 2H]^+$. These results and the poor solubility suggest the polymeric nature of the compound, which is composed of dithiolate and Xantphos ligated ionic species of Pd , formed after catalysis reaction. Interestingly, the powder X-ray diffraction (PXRD) pattern of the similar compound obtained after six catalysis cycles (Figure S37c), showed two broad peaks at $2\theta \sim 40.1$ and 44.6°, which may be attributed to the Pd-nanoparticles (PdNPs) (Powder Diffraction File no. 46–1043, Joint Committee on Powder Diffraction Standards, 1993), whereas the largest peak at $2\theta \sim 22.2°$ is possibly due to the bulk species present in the compound. The size of the PdNPs calculated using the Debye–Scherrer formula is ~3 nm. The PXRD pattern of the similar compound obtained after zero cycles also showed the highly broadened peak at $2\theta \sim 40.1°$ (Figure S37b). Perhaps the reducing atmosphere by the presence of solvent methanol, phosphine, and thiol ligands favor the formation of PdNPs.[52] A large number of Pd-containing metallocycles showed excellent catalytic efficiency in C–C coupling reactions, which have been established now due to the formation of active intermediate PdNPs as catalyst.[53,54] Others have reported that Pd clusters may also be generated with PdNPs, including the Pd complex, can interconvert to make the active catalytic system for the successful coupling of wide range of substrates as presently observed.[55,56] However, more investigations are required to establish the true nature of present catalyst.

CONCLUSIONS

In summary, we have successfully isolated Xantphos-blocked Pd(II) and Pt(II) complexes with bridging dithiol ligands by self-assembly. The reactions with 1,4-benezenedithiol or 4,4′-biphenyldithiol resulted in dinuclear complex **I** and tetranuclear complex **II**. The equilibrium between **I** and **II** has been established in platinum complexes of 4,4′-biphenyldithiolate, which lies at the side of **II**. In striking contrast, when we previously used the smaller bite angle dppe or triethyl phosphines as capping ligand, the analogous complexes were exclusively isolated as **II**. Steric crowding coupled with flexible coordination around the metal center is the primary reason to adopt such structures. By varying the positions of two thiol groups, employing 1,3-benezenedithiol, the same reactions lead to dinuclear complex **III**, containing a S–S bond between two thiolate ligands. The steric reason does not allow to form or stabilize to tetranuclear complex **II′** of 1,3-benezenedithiolate.

Moreover, the palladium complexes show excellent activity in Suzuki C–C cross coupling reactions under mild conditions. The catalytic systems can couple a wide range of aryl halides, giving high yields and TON and can be reused 8 times without losing significant yield. The HOMO–LUMO gap and stability increase in the order **III** > **II** > **I**, which reflects in their comparative catalytic activity. We have demonstrated the comparative catalytic activity of tetranuclear Pd complexes **II**

DOI: 10.1021/acs.inorgchem.8b02726
Inorg. Chem. XXXX, XXX, XXX–XXX

of bis-phosphines of varied bite angles, Xantphos, dppf, and dppe. The PdNPs with dithiolate and Xantphos ligated Pd, as poorly soluble bulk compound has been identified, after the catalysis reactions of the palladium complexes. Overall, the present Pd complexes showed improved catalytic activity than the dppe analogues. The positive charge and stronger metal−sulfur bond of the present type of complexes can make them capable as potential functional materials for other solution-based applications by modification of suitable capping ligand.

■ ASSOCIATED CONTENT

Supporting Information

The Supporting Information is available free of charge on the ACS Publication Web site at The Supporting Information is available free of charge on the ACS Publications website at DOI: 10.1021/acs.inorgchem.8b02726.

Details of general procedures of the experiments, crystallographic and structure refinement data tables of all complexes, tables of calculated and experimental ion peaks of the complexes, bond distances and angles of **2a**, percentage composition of frontier molecular orbitals of **3a-II** and **4a-II**, effect of bite angle of phosphine on catalysis of $[Pd_2(P^{\cap}P)_2(SC_{12}H_8S)]_2(OTf)_4$, ^1H and $^{31}P\{^1H\}$ NMR spectra of all the complexes, molecular structure of **2a**, $^{19}F\{^1H\}$ NMR spectrum of **3b**, VT ^1H NMR spectrum of **4b**, ESI-mass spectra of **3a**, **3b**, and **4a**, UV−vis spectra of **3b**, **4b**, and compound after catalytic reactions of **3b**, thermogravimetric curve of **3b**, X-ray structures of **2a** and **4c-III**, plots of HOMO and LUMO of **3a-II** and **4a-II**, PXRD pattern of **3b** before and after catalysis reaction, ^1H NMR spectra of all the biaryls as coupling products (PDF)

Accession Codes

CCDC 1865095−1865100 contain the supplementary crystallographic data for this paper. These data can be obtained free of charge via www.ccdc.cam.ac.uk/data_request/cif, or by emailing data_request@ccdc.cam.ac.uk, or by contacting The Cambridge Crystallographic Data Centre, 12 Union Road, Cambridge CB2 1EZ, UK; fax: +44 1223 336033.

■ AUTHOR INFORMATION

Corresponding Author

*Tel.: 91 22 25592589. E-mail: dsandip@barc.gov.in.

ORCID

Sandip Dey: 0000-0001-9198-8808

Arup Kumar Pathak: 0000-0002-5857-0132

Notes

The authors declare no competing financial interest.

■ ACKNOWLEDGMENTS

P.M. is thankful to the Department of Atomic Energy-Mumbai University Collaborative Scheme for providing senior research fellowship. We are grateful to the staff of Fuel Chemistry Division of BARC for providing the mass spectra.

■ REFERENCES

(1) Cook, T. R.; Vajpayee, V.; Lee, M. H.; Stang, P. J.; Chi, K.-W. Biomedical and Biochemical Applications of Self-Assembled Metallacycles and Metallacages. *Acc. Chem. Res.* **2013**, *46*, 2464−2474.

(2) Wiester, M. J.; Ulmann, P. A.; Mirkin, C. A. Enzyme Mimics based upon Supramolecular Coordination Chemistry. *Angew. Chem., Int. Ed.* **2011**, *50*, 114−137.

(3) Ghosh, S.; Mukherjee, P. S. Self-Assembly of a Nanoscopic Prism via a New Organometallic Pt_3 Acceptor and Its Fluorescent Detection of Nitroaromatics. *Organometallics* **2008**, *27*, 316−319.

(4) Cook, T. R.; Zheng, Y. R.; Stang, P. J. Metal−Organic Frameworks and Self-Assembled Supramolecular Coordination Complexes: Comparing and Contrasting the Design, Synthesis, and Functionality of Metal−Organic Materials. *Chem. Rev.* **2013**, *113*, 734−777.

(5) Hastings, C. J.; Pluth, M. D.; Bergman, R. G.; Raymond, K. N. Enzymelike Catalysis of the Nazarov Cyclization by Supramolecular Encapsulation. *J. Am. Chem. Soc.* **2010**, *132*, 6938−6940.

(6) Murase, T.; Horiuchi, S.; Fujita, M. Naphthalene Diels−Alder in a Self-Assembled Molecular Flask. *J. Am. Chem. Soc.* **2010**, *132*, 2866−2867.

(7) Vivekananda, K. V.; Dey, S.; Maity, D. K.; Bhuvanesh, N.; Jain, V. K. Supramolecular Macrocyclic Pd(II) and Pt(II) Squares and Rectangles with Aryldithiolate Ligands and their Excellent Catalytic Activity in Suzuki C−C Coupling Reaction. *Inorg. Chem.* **2015**, *54*, 10153−10162.

(8) Chand, D. K.; Biradha, K.; Kawano, M.; Sakamoto, S.; Yamaguchi, K.; Fujita, M. Dynamic Self-Assembly of an M_3L_6 Molecular Triangle and an M_4L_8 Tetrahedron from Naked Pd^{II} Ions and Bis(3-pyridyl)-Substituted Arenes. *Chem. - Asian J.* **2006**, *1−2*, 82−90.

(9) Tabellion, F. M.; Seidel, S.; Arif, A. M.; Stang, P. J. Discrete Supramolecular Architecture vs Crystal Engineering: The Rational Design of a Platinum-Based Bimetallic Assembly with a Chairlike Structure and Its Infinite, Copper Analogue. *J. Am. Chem. Soc.* **2001**, *123*, 7740−7741.

(10) Dey, S.; Vivekananda, K. V.; Bhuvanesh, N. Supramolecular Pt and Pd Complexes of 4,4'-Dipyridylditelluride/diselenide Ligands via Self-Assembly. *Eur. J. Inorg. Chem.* **2018**, *2018*, 3579−3586.

(11) Sun, Y.; Li, S.; Zhou, Z.; Saha, M. L.; Datta, S.; Zhang, M.; Yan, X.; Tian, D.; Wang, H.; Wang, L.; Li, X.; Liu, M.; Li, H.; Stang, P. J. Alanine-Based Chiral Metallogels via Supramolecular Coordination Complex Platforms: Metallogelation Induced Chirality Transfer. *J. Am. Chem. Soc.* **2018**, *140*, 3257−3263.

(12) Kieltyka, R.; Englebienne, P.; Fakhoury, J.; Autexier, C.; Moitessier, N.; Sleiman, H. F. A Platinum Supramolecular Square as an Effective G-Quadruplex Binder and Telomerase Inhibitor. *J. Am. Chem. Soc.* **2008**, *130*, 10040−10041.

(13) Grishagin, I. V.; Pollock, J. B.; Kushal, S.; Cook, T. R.; Stang, P. J.; Olenyuk, B. Z. In vivo anticancer activity of rhomboidal Pt(II) metallacycles. *Proc. Natl. Acad. Sci. U. S. A.* **2014**, *111*, 18448−18453.

(14) Samanta, D.; Mukherjee, S.; Patil, Y. P.; Mukherjee, P. S. Self-Assembled Pd_6 Open Cage with Triimidazole Walls and the Use of Its Confined Nanospace for Catalytic Knoevenagel- and Diels−Alder Reactions in Aqueous Medium. *Chem. - Eur. J.* **2012**, *18*, 12322−12329.

(15) Zhao, C.-W.; Ma, J.-P.; Liu, Q.-K.; Yu, Y.; Wang, P.; Li, Y.-A.; Wang, K.; Dong, Y.-B. A self-assembled Pd_6L_8 nanoball for Suzuki−Miyaura coupling reactions in both homogeneous and heterogeneous formats. *Green Chem.* **2013**, *15*, 3150−3154.

(16) Vivekananda, K. V.; Dey, S.; Wadawale, A.; Bhuvanesh, N.; Jain, V. K. Supramolecular 3-/4-Mercaptobenzoic Acid Complexes of Palladium(II) and Platinum(II) Stabilized by Hydrogen Bonding. *Eur. J. Inorg. Chem.* **2014**, *2014*, 2153−2161.

(17) Mane, P. A.; Dey, S.; Vivekananda, K. V. Macrocyclic Pd(II) dithiolate complexes as catalysts in Heck reactions. *Tetrahedron Lett.* **2017**, *58*, 25−29.

(18) Fujita, M.; Sasaki, O.; Mitsuhashi, T.; Fujita, T.; Yazaki, J.; Yamaguchi, K.; Ogura, K. On the structure of transition-metal-linked molecular squares. *Chem. Commun.* **1996**, 1535−1536.

(19) Zhang, L.; Niu, Y.-H.; Jen, A. K.-Y.; Lin, W. A Highly Electroluminescent Molecular Square. *Chem. Commun.* **2005**, 1002−1004.

DOI: 10.1021/acs.inorgchem.8b02726
Inorg. Chem. XXXX, XXX, XXX−XXX

(20) Liron, F.; Fosse, C.; Pernolet, A.; Roulland, E. Suzuki−Miyaura Cross-Coupling of 1,1-Dichloro-1-alkenes with 9-Alkyl-9-BBN. *J. Org. Chem.* **2007**, *72*, 2220−2223.
(21) Van Haaren, R. J.; Goubitz, K.; Fraanje, J.; Van Strijdonck, G. P. F.; Oevering, H.; Coussens, B.; Reek, J. N. H.; Kamer, P. C. J.; Van Leeuwen, P. W. N. M. X-ray Study of the Effect of the Bite Angle of Chelating Ligands on the Geometry of Palladium(allyl) Complexes: Implications for the Regioselectivity in the Allylic Alkylation. *Inorg. Chem.* **2001**, *40*, 3363−3372.
(22) Wagaw, S.; Yang, B. H.; Buchwald, S. L. A Palladium-Catalyzed Method for the Preparation of Indoles via the Fischer Indole Synthesis. *J. Am. Chem. Soc.* **1999**, *121*, 10251−10263.
(23) Gao, G.-Y.; Colvin, A. J.; Chen, Y.; Zhang, X. P. Versatile Synthesis of meso-Aryloxy- and Alkoxy-Substituted Porphyrins via Palladium-Catalyzed C−O Cross-Coupling Reactions. *Org. Lett.* **2003**, *5*, 3261−3264.
(24) Van der Veen, L. A.; Keeven, P. H.; Schoemaker, G. C.; Reek, J. N. H.; Kamer, P. C. J.; Van Leeuwen, P. W. N. M.; Lutz, M.; Spek, A. L. Origin of the Bite Angle Effect on Rhodium Diphosphine Catalyzed Hydroformylation. *Organometallics* **2000**, *19*, 872−883.
(25) Johns, A. M.; Utsunomiya, M.; Incarvito, C. D.; Hartwig, J. F. A Highly Active Palladium Catalyst for Intermolecular Hydroamination. Factors that Control Reactivity and Additions of Functionalized Anilines to Dienes and Vinylarene. *J. Am. Chem. Soc.* **2006**, *128*, 1828−1839.
(26) Yu, H.; Zhang, G.; Huang, H. Palladium-Catalyzed Dearomative Cyclocarbonylation by C−N Bond Activation. *Angew. Chem., Int. Ed.* **2015**, *54*, 10912−10916.
(27) Dierkes, P.; van Leeuwen, P. W. N. M. The bite angle makes the difference: a practical ligand parameter for diphosphine ligands. *J. Chem. Soc., Dalton Trans.* **1999**, 1519−1529.
(28) Gun, K.-S.; Hor, T. S. A. 1.1′-Bis(diphenylphosphino)ferrocene - Coordination Chemistry, Organic Syntheses and Catalysis. In *Ferrocenes: Homogeneous Catalysis, Organic Synthesis, Materials Science*, Togni, A., Hayashi, T., Ed.; Wiley-VCH: New York, 1995; Chapter 1, p 31.
(29) Becke, A. D. Density-functional exchange-energy approximation with correct asymptotic behavior. *Phys. Rev. A: At., Mol., Opt. Phys.* **1988**, *38*, 3098−3100.
(30) Perdew, J. P. Density-functional approximation for the correlation energy of the inhomogeneous electron gas. *Phys. Rev. B: Condens. Matter Mater. Phys.* **1986**, *33*, 8822−8824.
(31) Su, P.; Li, H. Energy decomposition analysis of covalent bonds and intermolecular interactions. *J. Chem. Phys.* **2009**, *131*, 014102.
(32) Schmidt, M. W.; Baldridge, K. K.; Boatz, J. A.; Elbert, S. T.; Gordon, M. S.; Jensen, J. H.; Koseki, S.; Matsunaga, N.; Nguyen, K. A.; Su, S.; Windus, T. L.; Dupuis, M.; Montgomery, J. A. General atomic and molecular electronic structure system. *J. Comput. Chem.* **1993**, *14*, 1347−1363.
(33) Schaftenaar, G.; Noordik, J. H. Molden: a pre- and post-processing program for molecular and electronic structures. *J. Comput.-Aided Mol. Des.* **2000**, *14*, 123−134.
(34) Portmann, S.; Luthi, H. MOLEKEL: An Interactive Molecular Graphics Tool. *Chimia* **2000**, *54*, 766−770.
(35) Martinelli, J. R.; Watson, D. A.; Freckmann, D. M. M.; Barder, T. E.; Buchwald, S. L. Palladium-Catalyzed Carbonylation Reactions of Aryl Bromides at Atmospheric Pressure: A General System Based on Xantphos. *J. Org. Chem.* **2008**, *73*, 7102−7107.
(36) Ji, Y.; Plata, R. E.; Regens, C. S.; Hay, M.; Schmidt, M.; Razler, T.; Qiu, Y.; Geng, P.; Hsiao, Y.; Rosner, T.; Eastgate, M. D.; Blackmond, D. G. Mono-Oxidation of Bidentate Bis-phosphines in Catalyst Activation: Kinetic and Mechanistic Studies of a Pd/Xantphos-Catalyzed C−H Functionalization. *J. Am. Chem. Soc.* **2015**, *137*, 13272−13281.
(37) Capdevila, M.; Clegg, W.; González-Duarte, P.; Jarid, A.; Lledós, A. Hinge Distortion in Platinum(II) Dimers with a Pt_2S_2 Ring. An ab Initio Molecular Orbital Study. *Inorg. Chem.* **1996**, *35*, 490−497.
(38) Tang, R. P-L.; Wong, K. M-C.; Zhu, N.; Yam, V.W.-W. Luminescence, electrochemistry and host−guest properties of dinuclear platinum(II) terpyridyl complexes of sulfur-containing bridging ligands. *Dalton Trans.* **2009**, 3911−3922.
(39) Dolomanov, O. V.; Bourhis, L. J.; Gildea, R. J.; Howard, J. A. K.; Puschmann, H. *OLEX2*A Complete Structure Solution, Refinement and Analysis Program. *J. Appl. Crystallogr.* **2009**, *42*, 339−341.
(40) Ehlich, H.; Schier, A.; Schmidbaur, H. Aurophilicity-Based One-Dimensional Arrays of Gold(I) Phenylene-1,3- and −1,4-dithiolates. *Inorg. Chem.* **2002**, *41*, 3721−3727.
(41) Briant, C. E.; Calhorda, M. J.; Hor, T. S. A.; Howells, N. D.; Mingos, D. M. P. Chemistry of platinum sulphido-complexes. Part 3. Crystal and molecular structure of tetrasulphido[1,2-bis-(diphenylphosphino)ethane]platinum(II) and a study of its bonding and reactions. *J. Chem. Soc., Dalton Trans.* **1983**, 1325−1330.
(42) Rivera, G.; Bernes, S.; Torrens, H. Mono- and bimetallic platinum(II) and palladium(II) complexes containing fluorinated benzothiolates. *Polyhedron* **2007**, *26*, 4276−4286.
(43) Smith, V. C. M.; Aplin, R. T.; Brown, J. M.; Hursthouse, M. B.; Karalulov, A. I.; Malik, K. M. A.; Cooley, N. A. Scope of the C-S Insertion Reaction of Thiazolium Salts with Platinum(0) Diphosphine Complexe. *J. Am. Chem. Soc.* **1994**, *116*, 5180−5189.
(44) Niksch, T.; Görls, H.; Friedrich, M.; Oilunkaniemi, R.; Laitinen, R.; Weigand, W. The Extension of the Solid-Angle Concept to Bidentate Ligands. *Eur. J. Inorg. Chem.* **2010**, *2010*, 74−94.
(45) Ohshima, T.; Miyamoto, Y.; Ipposhi, J.; Nakahara, Y.; Utsunomiya, M.; Mashima, K. Platinum-Catalyzed Direct Amination of Allylic Alcohols under Mild Conditions: Ligand and Microwave Effects, Substrate Scope, and Mechanistic Study. *J. Am. Chem. Soc.* **2009**, *131*, 14317−14328.
(46) Kranenburg, M.; Delis, J. G. P.; Kamer, P. C. J.; van Leeuwen, P. W. N. M.; Vrieze, K.; Veldman, N.; Spek, A. L.; Goubitz, K.; Fraanje, J. Palladium(0)−tetracyanoethylene complexes of diphosphines and a dipyridine with large bite angles, and their crystal structures. *J. Chem. Soc., Dalton Trans.* **1997**, 1839−1849.
(47) Ferrer, M.; Mounir, M.; Rossell, O.; Ruiz, E.; Maestro, M. A. Equilibria between Metallosupramolecular Squares and Triangles with the New Rigid Linker 1,4-Bis(4-pyridyl)tetrafluorobenzene. Experimental and Theoretical Study of the Structural Dependence of NMR Data. *Inorg. Chem.* **2003**, *42*, 5890.
(48) Phua, P. H.; White, J. P.; de Vries, J. G.; Hii, K. K. Enabling Ligand Screening for Palladium-Catalysed Enantioselective Aza-Michael Addition Reactions. *Adv. Synth. Catal.* **2006**, *348*, 587.
(49) Magano, J.; Dunetz, J. R. Large-Scale Applications of Transition Metal-Catalyzed Couplings for the Synthesis of Pharmaceuticals. *Chem. Rev.* **2011**, *111*, 2177−2250.
(50) Proutiere, F.; Schoenebeck, F. Solvent Effect on Palladium Catalyzed Cross Coupling Reactions and Implications on the Active Catalytic Species. *Angew. Chem., Int. Ed.* **2011**, *50*, 8192−8195.
(51) Wang, W.-C.; Peng, K.-F.; Chen, M. − T.; Chen, C.−T. Palladacycles bearing tridentate CNS-type benzamidinate ligands as catalysts for cross-coupling reactions. *Dalton Trans.* **2012**, *41*, 3022−3029.
(52) Lu, C. -H; Chang, F.-C. Polyhedral Oligomeric Silsesquioxane-Encapsulating Amorphous Palladium Nanoclusters as Catalysts for Heck Reactions. *ACS Catal.* **2011**, *1*, 481−488.
(53) Louie, J.; Hartwig, J. F. A Route to Pd° from Pd^{II} Metallacycles in Animation and Cross Coupling Chemistry. *Angew. Chem., Int. Ed. Engl.* **1996**, *35*, 2359−2361.
(54) Astruc, D. Palladium Nanoparticles as Efficient Green Homogeneous and Heterogeneous Carbon−Carbon Coupling Precatalysts: A Unifying View. *Inorg. Chem.* **2007**, *46*, 1884−1894.
(55) Ananikov, V. P.; Beletskaya, I. P. Toward the Ideal Catalyst: From Atomic Centers to a "Cocktail" of Catalysts. *Organometallics* **2012**, *31*, 1595−1604.
(56) Eremin, D. B.; Ananikov, V. P. Understanding active species in catalytic transformations: From molecular catalysis to nanoparticles, leaching, "Cocktails" of catalysts and dynamic systems. *Coord. Chem. Rev.* **2017**, *346*, 2−19.

DOI: 10.1021/acs.inorgchem.8b02726
Inorg. Chem. XXXX, XXX, XXX−XXX